

Sequential Reaction Intermediates in Aliphatic C–H Bond Functionalization Initiated by a Bis(μ -oxo)dinickel(III) Complex

Jaeheung Cho,[†] Hideki Furutachi,[†] Shuhei Fujinami,[†] Takehiko Tosha,[‡] Hideki Ohtsu,[§] Osamu Ikeda,[†] Akane Suzuki,[⊥] Masaharu Nomura,[⊥] Tomoya Uruga,^{||} Hajime Tanida,^{||} Toshihide Kawai,^{||} Koji Tanaka,[§] Teizo Kitagawa,[‡] and Masatsugu Suzuki^{*†}

Department of Chemistry, Faculty of Science, Kanazawa University, Kakuma-machi, Kanazawa 920-1192, Japan, Okazaki Institute for Integrative Bioscience and Okazaki Institute for Molecular Science, National Institutes of Natural Sciences, 5-1 Higashiyama, Myodaiji, Okazaki 444-8787, Japan, Photon Factory, Institute of Materials Structure Science, High Energy Accelerator Research Organization, Oho, Tsukuba 305-0801, Japan, and SPring-8, Japan Synchrotron Radiation Research Institute, Mikazuki, Hyogo 679-5198, Japan

Received August 21, 2005

The reaction of $[\text{Ni}_2(\text{OH})_2(\text{Me}_2\text{-tpa})_2]^{2+}$ (**1**) ($\text{Me}_2\text{-tpa}$ = bis(6-methyl-2-pyridylmethyl)(2-pyridylmethyl)amine) with H_2O_2 causes oxidation of a methylene group on the $\text{Me}_2\text{-tpa}$ ligand to give an N-dealkylated ligand and oxidation of a methyl group to afford a ligand-based carboxylate and an alkoxide as the final oxidation products. A series of sequential reaction intermediates produced in the oxidation pathways, a bis(μ -oxo)dinickel(III) ($[\text{Ni}_2(\text{O})_2(\text{Me}_2\text{-tpa})_2]^{2+}$ (**2**)), a bis(μ -superoxo)dinickel(II) ($[\text{Ni}_2(\text{O}_2)_2(\text{Me}_2\text{-tpa})_2]^{2+}$ (**3**)), a (μ -hydroxo)(μ -alkylperoxo)dinickel(II) ($[\text{Ni}_2(\text{OH})(\text{Me}_2\text{-tpa})(\text{Me-tpa-CH}_2\text{OO})]^{2+}$ (**4**)), and a bis(μ -alkylperoxo)dinickel(II) ($[\text{Ni}_2(\text{Me-tpa-CH}_2\text{OO})_2]^{2+}$ (**5**)), was isolated and characterized by various physicochemical measurements including X-ray crystallography, and their oxidation pathways were investigated. Reaction of **1** with H_2O_2 in methanol at -40 °C generates **2**, which is extremely reactive with H_2O_2 , producing **3**. Complex **2** was isolated only from disproportionation of the superoxo ligands in **3** in the absence of H_2O_2 at -40 °C. Thermal decomposition of **2** under N_2 generated an N-dealkylated ligand Me-dpa ((6-methyl-2-pyridylmethyl)(2-pyridylmethyl)amine) and a ligand-coupling dimer $(\text{Me-tpa-CH}_2)_2$. The formation of $(\text{Me-tpa-CH}_2)_2$ suggests that a ligand-based radical $\text{Me-tpa-CH}_2^\bullet$ is generated as a reaction intermediate, probably produced by H-atom abstraction by the oxo group. An isotope-labeling experiment revealed that intramolecular coupling occurs for the formation of the coupling dimer. The results indicate that the rebound of oxygen to $\text{Me-tpa-CH}_2^\bullet$ is slower than that observed for various high-valence bis(μ -oxo)dimetal complexes. In contrast, the decomposition of **2** and **3** in the presence of O_2 gave carboxylate and alkoxide ligands, respectively (Me-tpa-COO^- and $\text{Me-tpa-CH}_2\text{O}^-$), instead of $(\text{Me-tpa-CH}_2)_2$, indicating that the reaction of $\text{Me-tpa-CH}_2^\bullet$ with O_2 is faster than the coupling of $\text{Me-tpa-CH}_2^\bullet$ to generate ligand-based peroxy radical $\text{Me-tpa-CH}_2\text{OO}^\bullet$. Although there is a possibility that the $\text{Me-tpa-CH}_2\text{OO}^\bullet$ species could undergo various reactions, one of the possible reactive intermediates, **4**, was isolated from the decomposition of **3** under O_2 at -20 °C. The alkylperoxo ligands in **4** and **5** can be converted to a ligand-based aldehyde by either homolysis or heterolysis of the O–O bond, and disproportionation of the aldehyde gives a carboxylate and an alkoxide via the Cannizzaro reaction.

Introduction

Oxidation reactions mediated by metal complexes with various active-oxygen species M_m/O_n such as superoxo,

* To whom correspondence should be addressed. E-mail: suzuki@cacheibm.s.kanazawa-u.ac.jp. Phone: 81-76-264-5701. Fax: 81-76-264-5742.

[†] Kanazawa University.

[‡] Okazaki Institute for Integrative Bioscience, National Institutes of Natural Sciences.

peroxo, and high-valence bis(μ -oxo)dimetal complexes are of great importance for understanding the reaction mechanisms of nonheme metalloenzymes and for utilizing metal complexes as oxidation catalysts.^{1–6} A variety of synthetic

[§] Okazaki Institute for Molecular Science, National Institutes of Natural Sciences.

[⊥] Institute of Materials Structure Science.

^{||} Japan Synchrotron Radiation Research Institute.

high-valence bis(μ -oxo)dimetal complexes ($M = \text{Fe}^{4,7,8}$ and $\text{Cu}^{6,9-13}$) have been developed. They provide a chemical basis

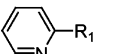
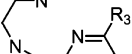
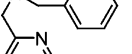
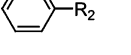
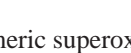
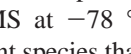
for understanding the structural and various spectroscopic properties and reactivities of high-valence bis(μ -oxo)dimetal complexes. Some of these complexes have been shown to be key intermediates for the aliphatic hydroxylation.

Such high-valence bis(μ -oxo)dimetal chemistry has been extended to Co and Ni complexes by Hikichi and co-workers.^{14,15} Various types of bis(μ -oxo)dinickel(III) complexes have been developed using tridentate and tetradentate ligands.¹⁴⁻²⁰ Some of these are capable of aliphatic ligand hydroxylation via H-atom abstraction by the oxo group in $\text{Ni}^{\text{III}}(\mu\text{-O})_2\text{Ni}^{\text{III}}$. It was found that the reactivity of a bis(μ -oxo)dinickel(III) complex that has tetradentate tripod ligand $\text{Me}_3\text{-tpa}$ $[\text{Ni}_2(\text{O})_2(\text{Me}_3\text{-tpa})_2]^{2+}$ ($2^{\text{Me}_3\text{-tpa}}$) is quite different from that of the complexes with tridentate ligands; $2^{\text{Me}_3\text{-tpa}}$ reacts with H_2O_2 to generate a bis(μ -superoxo)dinickel(II) complex $[\text{Ni}_2(\text{O})_2(\text{Me}_3\text{-tpa})_2]^{2+}$ ($3^{\text{Me}_3\text{-tpa}}$), which can be converted into $2^{\text{Me}_3\text{-tpa}}$ and O_2 by disproportionation.¹⁷ Furthermore, decomposition of $2^{\text{Me}_3\text{-tpa}}$ and $3^{\text{Me}_3\text{-tpa}}$ under O_2 produced a ligand-based carboxylate (Me-tpa-COO^-) and an alcohol ($\text{Me-tpa-CH}_2\text{OH}$) in which the carboxylate ligand is not derived from the autoxidation of the alkoxide ligand under the conditions; some other reaction pathways have been suggested.

Recently, we found that the 6-methyl group of the pyridyl group of $\text{Me}_n\text{-tpa}$ derivatives significantly influences the reactivity of a bis(μ -hydroxo)dinickel(II) complex with H_2O_2 ; reaction of $[\text{Ni}_2(\text{OH})_2(\text{Me}_2\text{-tpa})_2]^{2+}$ (**1**) with H_2O_2 produced a ligand-based bis(μ -alkylperoxo)dinickel(II) complex $[\text{Ni}_2(\text{Me-tpa-CH}_2\text{OO})_2]^{2+}$ (**5**) at -20°C .²¹ Unlike in the $\text{Me}_3\text{-tpa}$ system, no bis(μ -oxo)dinickel(III) species $[\text{Ni}_2(\text{O})_2(\text{Me}_2\text{-tpa})_2]^{2+}$ (**2**) was detected in the presence of H_2O_2 , but a

- (1) (a) Simándi, L. I., Ed. *Catalytic Activation of Dioxygen by Metal Complexes*; Kluwer Academic Publishers: Dordrecht, The Netherlands, 1992. (b) Meunier, B., Ed. *Biomimetic Oxidations Catalyzed by Transition Metal Complexes*; Imperial College Press: London, 1999. (c) Reedijk, J., Bouwman, E., Eds. *Bioinorganic Catalysis*, 2nd ed.; Marcel Dekker: New York, 1999.
- (2) (a) Solomon, E. I.; Brunold, T. C.; Davis, M. I.; Kemsley, J. N.; Lee, S.-K.; Lehnert, N.; Neese, F.; Skulan, A. J.; Yang, Y.-S.; Zhou, J. *Chem. Rev.* **2000**, *100*, 235. (b) Merckx, M.; Kopp, D. A.; Sazinsky, M. H.; Blazyk, J. L.; Müller, J.; Lippard, S. J. *Angew. Chem., Int. Ed.* **2001**, *40*, 2782. (c) Baik, M.-H.; Newcomb, M.; Friesner, R. A.; Lippard, S. J. *Chem. Rev.* **2003**, *103*, 2385. (d) Fox, B. G.; Lyle, K. S.; Rogge, C. E. *Acc. Chem. Res.* **2004**, *37*, 421.
- (3) (a) Solomon, E. I.; Sundaram, U. M.; Machonkin, T. E. *Chem. Rev.* **1996**, *96*, 2563. (b) Klinman, J. P. *Chem. Rev.* **1996**, *96*, 2541. (c) Solomon, E. I.; Chen, P.; Metz, M.; Lee, S.-K.; Palmer, A. E. *Angew. Chem., Int. Ed.* **2001**, *40*, 4570. (d) Whittaker, J. W. *Chem. Rev.* **2003**, *103*, 2347.
- (4) (a) Que, L., Jr. *J. Chem. Soc., Dalton Trans.* **1997**, 3933. (b) Que, L., Jr.; Tolman, W. B. *Angew. Chem., Int. Ed.* **2002**, *41*, 1114. (c) Bois, J. D.; Mizoguchi, T. J.; Lippard, S. J. *Coord. Chem. Rev.* **2000**, *200-202*, 443. (d) Tshuva, E. Y.; Lippard, S. J. *Chem. Rev.* **2004**, *104*, 987.
- (5) (a) Costas, M.; Chen, K.; Que, L., Jr. *Coord. Chem. Rev.* **2000**, *200-202*, 517. (b) Chen, K.; Costas, M.; Que, L., Jr. *J. Chem. Soc., Dalton Trans.* **2002**, 672. (c) Costas, M.; Mehn, M. P.; Jensen, M. P.; Que, L., Jr. *Chem. Rev.* **2004**, *104*, 939.
- (6) (a) Tolman, W. B. *Acc. Chem. Res.* **1997**, *30*, 227. (b) Holland, P. L.; Tolman, W. B. *Coord. Chem. Rev.* **1999**, *190-192*, 855. (c) Itoh, S.; Fukuzumi, S. *Bull. Chem. Soc. Jpn.* **2002**, *75*, 2081. (d) Mirica, L. M.; Ottenwaelder, X.; Stack, T. D. P. *Chem. Rev.* **2004**, *104*, 1013. (e) Lewis, E. A.; Tolman, W. B. *Chem. Rev.* **2004**, *104*, 1047. (f) Hatcher, L. Q.; Karlin, K. D. *J. Biol. Inorg. Chem.* **2004**, *9*, 669.
- (7) (a) Dong, Y.; Fujii, H.; Hendrich, M. P.; Leising, R. A.; Pan, G.; Randall, C. R.; Wilkinson, E. C.; Zang, Y.; Que, L., Jr.; Fox, B. G.; Kauffmann, K.; Münck, E. J. *Am. Chem. Soc.* **1995**, *117*, 2778. (b) Dong, Y.; Zang, Y.; Kauffmann, K.; Shu, L.; Wilkinson, E. C.; Münck, E.; Que, L., Jr. *J. Am. Chem. Soc.* **1997**, *119*, 12683. (c) Hsu, H.-F.; Dong, Y.; Shu, L.; Young, V. G., Jr.; Que, L., Jr. *J. Am. Chem. Soc.* **1999**, *121*, 5230. (d) Lee, D.; Bois, J. D.; Petasis, D.; Hendrich, M. P.; Krebs, C.; Huynh, B. H.; Lippard, S. J. *J. Am. Chem. Soc.* **1999**, *121*, 9893. (e) Lee, D.; Pierce, B.; Krebs, C.; Hendrich, M. P.; Huynh, B. H.; Lippard, S. J. *J. Am. Chem. Soc.* **2002**, *124*, 3993. (f) Skulan, A. J.; Hanson, M. A.; Hsu, H.-f.; Que, L., Jr.; Solomon, E. I. *J. Am. Chem. Soc.* **2003**, *125*, 7344.
- (8) Costas, M.; Rohde, J.-U.; Stubna, A.; Ho, R. Y. N.; Quaroni, L.; Münck, E.; Que, L., Jr. *J. Am. Chem. Soc.* **2001**, *123*, 12931.
- (9) (a) Halfen, J. A.; Mahapatra, S.; Wilkinson, E. C.; Kaderli, S.; Young, V. G., Jr.; Que, L., Jr.; Zuberbühler, A. D.; Tolman, W. B. *Science* **1996**, *271*, 1397. (b) Cole, A. P.; Root, D. E.; Mukherjee, P.; Solomon, E. I.; Stack, T. D. P. *Science* **1996**, *273*, 1848. (c) Mahapatra, S.; Halfen, J. A.; Wilkinson, E. C.; Pan, G.; Wang, X.; Young, V. G., Jr.; Cramer, C. J.; Que, L., Jr.; Tolman, W. B. *J. Am. Chem. Soc.* **1996**, *118*, 11555. (d) Mahadevan, V.; Hou, Z.; Cole, A. P.; Root, D. E.; Lal, T. K.; Solomon, E. I.; Stack, T. D. P. *J. Am. Chem. Soc.* **1997**, *119*, 11996. (e) Mahapatra, S.; Young, V. G.; Kaderli, S.; Zuberbühler, A. D.; Tolman, W. B. *Angew. Chem., Int. Ed.* **1997**, *36*, 130. (f) Hayashi, H.; Fujinami, S.; Nagatomo, S.; Ogo, S.; Suzuki, M.; Uehara, A.; Watanabe, Y.; Kitagawa, T. *J. Am. Chem. Soc.* **2000**, *122*, 2124. (g) Straub, B. F.; Rominger, F.; Hofmann, P. *J. Chem. Soc., Chem. Commun.* **2000**, 1611. (h) Aboelella, N. W.; Lewis, E. A.; Reynolds, A. M.; Brennessel, W. W.; Cramer, C. J.; Tolman, W. B. *J. Am. Chem. Soc.* **2002**, *124*, 10660. (i) Mizuno, M.; Hayashi, H.; Fujinami, S.; Furutachi, H.; Nagatomo, S.; Otake, S.; Uozumi, K.; Suzuki, M.; Kitagawa, T. *Inorg. Chem.* **2003**, *42*, 8534.
- (10) (a) Mahapatra, S.; Halfen, J. A.; Tolman, W. B. *J. Am. Chem. Soc.* **1996**, *118*, 11575. (b) Holland, P. L.; Rodgers, K. R.; Tolman, W. B. *Angew. Chem., Int. Ed.* **1999**, *38*, 1139. (c) Itoh, S.; Taki, M.; Nakao, H.; Holland, P. L.; Tolman, W. B.; Que, L., Jr.; Fukuzumi, S. *Angew. Chem., Int. Ed.* **2000**, *39*, 398.
- (11) (a) Mahadevan, V.; DuBois, J. L.; Hedman, B.; Hodgson, K. O.; Stack, T. D. P. *J. Am. Chem. Soc.* **1999**, *121*, 5583. (b) Taki, M.; Itoh, S.; Fukuzumi, S. *J. Am. Chem. Soc.* **2001**, *123*, 6203. (c) Taki, M.; Itoh, S.; Fukuzumi, S. *J. Am. Chem. Soc.* **2002**, *124*, 998. (d) Osako, T.; Ohkubo, K.; Taki, M.; Tachi, Y.; Fukuzumi, S.; Itoh, S. *J. Am. Chem. Soc.* **2003**, *125*, 11027. (e) Shearer, J.; Zhang, C. X.; Zakhharov, L. N.; Rheingold, A. L.; Karlin, K. D. *J. Am. Chem. Soc.* **2005**, *127*, 5469.
- (12) (a) Cahoy, J.; Holland, P. L.; Tolman, W. B. *Inorg. Chem.* **1999**, *38*, 2161. (b) Pidcock, E.; DeBeer, S.; Obias, H. V.; Hedman, B.; Hodgson, K. O.; Karlin, K. D.; Solomon, E. I. *J. Am. Chem. Soc.* **1999**, *121*, 1870. (c) Mahadevan, V.; Henson, M. J.; Solomon, E. I.; Stack, T. D. P. *J. Am. Chem. Soc.* **2000**, *122*, 10249. (d) Liang, H.-C.; Zhang, C. X.; Henson, M. J.; Sommer, R. D.; Hatwell, K. R.; Kaderli, S.; Zuberbühler, A. D.; Rheingold, A. L.; Solomon, E. I.; Karlin, K. D. *J. Am. Chem. Soc.* **2002**, *124*, 4170. (e) Taki, M.; Teramae, S.; Nagatomo, S.; Tachi, Y.; Kitagawa, T.; Itoh, S.; Fukuzumi, S. *J. Am. Chem. Soc.* **2002**, *124*, 6367.
- (13) (a) Henson, M. J.; Mukherjee, P.; Root, D. E.; Stack, T. D. P.; Solomon, E. I. *J. Am. Chem. Soc.* **1999**, *121*, 10332. (b) Holland, P. L.; Cramer, C. J.; Wilkinson, E. C.; Mahapatra, S.; Rodgers, K. R.; Itoh, S.; Taki, M.; Fukuzumi, S.; Que, L., Jr.; Tolman, W. B. *J. Am. Chem. Soc.* **2000**, *122*, 792.
- (14) (a) Hikichi, S.; Akita, M.; Moro-oka, Y. *Coord. Chem. Rev.* **2000**, *198*, 61. (b) Akita, M.; Hikichi, S. *Bull. Chem. Soc. Jpn.* **2002**, *75*, 1657.
- (15) (a) Hikichi, S.; Yoshizawa, M.; Sasakura, Y.; Akita, M.; Moro-oka, Y. *J. Am. Chem. Soc.* **1998**, *120*, 10567. (b) Hikichi, S.; Yoshizawa, M.; Sasakura, Y.; Komatsuzaki, H.; Moro-oka, Y.; Akita, M. *Chem-Eur. J.* **2001**, *7*, 5011.
- (16) (a) Itoh, S.; Bandoh, H.; Nagatomo, S.; Kitagawa, T.; Fukuzumi, S. *J. Am. Chem. Soc.* **1999**, *121*, 8945. (b) Itoh, S.; Bandoh, H.; Nakagawa, M.; Nagatomo, S.; Kitagawa, T.; Karlin, K. D.; Fukuzumi, S. *J. Am. Chem. Soc.* **2001**, *123*, 11168.
- (17) Shiren, K.; Ogo, S.; Fujinami, S.; Hayashi, H.; Suzuki, M.; Uehara, A.; Watanabe, Y.; Moro-oka, Y. *J. Am. Chem. Soc.* **2000**, *122*, 254.
- (18) Mandimutsira, B. S.; Yamarik, J. L.; Brunold, T. C.; Gu, W.; Cramer, S. P.; Riordan, C. G. *J. Am. Chem. Soc.* **2001**, *123*, 9194.
- (19) Fujita, K.; Schenker, R.; Gu, W.; Brunold, T. C.; Cramer, S. P.; Riordan, C. G. *Inorg. Chem.* **2004**, *43*, 3324.
- (20) Schenker, R.; Mandimutsira, B. S.; Riordan, C. G.; Brunold, T. C. *J. Am. Chem. Soc.* **2002**, *124*, 13842.
- (21) Cho, J.; Furutachi, H.; Fujinami, S.; Suzuki, M. *Angew. Chem., Int. Ed.* **2004**, *43*, 3300.

Chart 1

	R ₁	R ₂	R ₃
	CH ₃	CH ₃	CH ₃
	CH ₃	CH ₃	H
	CH ₃	CH ₂ OH	H
	CH ₃	CHO	H
	CH ₃	CH ₂ OO ⁻	H
	CH ₃	COO ⁻	H

monomeric superoxonickel(II) species was detected by ESI-TOF/MS at -78 °C, suggesting the existence of **2** as a transient species that could be extremely reactive with H₂O₂, generating the superoxo species. It was also found that the alkylperoxo ligands of **5** are further converted into Me-tpa-COO⁻ and Me-tpa-CH₂OH. Isotope-labeling experiments suggested that either homolysis or heterolysis of the O–O bond of the alkylperoxide generates a ligand-based aldehyde, Me-tpa-CHO, which is further converted into Me-tpa-COO⁻ and Me-tpa-CH₂OH via the Cannizzaro reaction. Thus, the reaction of **1** with H₂O₂ involves rich oxidation chemistry.

In this study, we have investigated the formation pathways of **5** initiated by the reaction of **1** with H₂O₂ and the oxidation pathways of the supporting ligand. The sequential reaction intermediates generated in the oxidation pathways, bis(μ -oxo)nickel(III) ([Ni₂(O)₂(Me₂-tpa)₂]²⁺ (**2**)), bis(μ -superoxo)nickel(II) ([Ni₂(O₂)₂(Me₂-tpa)₂]²⁺ (**3**)), (μ -hydroxo)-(μ -alkylperoxo)nickel(II) ([Ni₂(OH)(Me₂-tpa)(Me-tpa-CH₂-OO)]²⁺ (**4**)), and bis(μ -alkylperoxo)nickel(II) ([Ni₂(Me-tpa-CH₂OO)₂]²⁺ (**5**)), were successfully isolated and characterized by various physicochemical measurements, including X-ray crystallography. The formation and oxidation reactions of the above complexes containing active-oxygen species were investigated in comparison with those of the corresponding Me₃-tpa complexes (see Chart 1).

Experimental Section

Materials. Me₃-tpa, Me₂-tpa, and Me-tpa were prepared according to the literature methods.²² H₂¹⁸O₂ was prepared by the literature methods.²³ Acetonitrile and acetone were dried over 5 Å molecular sieves and distilled under a N₂ atmosphere before use.

Synthesis of Ligand *d*₁-Me₂-tpa. A methanol solution (50 mL) of 2-(aminomethyl)pyridine (4.806 g, 44 mmol) was added to a methanol solution (50 mL) of 6-methylpyridine-2-aldehyde (4.845 g, 40 mmol). To the resulting solution was slowly added NaBD₄ (1.848 g, 44 mmol) with stirring at room temperature. After the solution was stirred for a day, HCl was added until the pH of the solution became 1 in order to decompose an excess of NaBD₄. An aqueous solution of NaOH was added to make the solution basic, and the solution was concentrated under reduced pressure to remove methanol. The resulting solution was extracted with Et₂O (3 × 100 mL). The combined extracts were dried over Na₂SO₄, and Et₂O was removed by evaporation under reduced pressure. The residue was dissolved into a THF solution (100 mL) of 6-methylpyridine-2-aldehyde (4.845 g, 40 mmol). NaBH(CH₃CO₂)₃ (9.613 g, 44 mmol) was slowly added to the solution. After the solution was stirred for a day, HCl was added until the pH of the solution became

1 in order to decompose an excess of NaBH(CH₃CO₂)₃. An aqueous solution of NaOH was added to make the solution basic, and the solution was concentrated under reduced pressure to remove THF. The resulting solution was extracted with Et₂O (3 × 100 mL). The combined extracts were dried over Na₂SO₄, and Et₂O was removed by evaporation under reduced pressure to give a yellow oil of *d*₁-Me₂-tpa. ¹H NMR (CDCl₃, 300 MHz): δ 2.52 (6H, s, CH₃), 3.83 (1H, s, CDH), 3.86 (2H, s, CH₂), 3.88 (2H, s, CH₂), 6.99 (2H, d, pyH), 7.13 (1H, t, pyH), 7.42 (2H, d, pyH), 7.53 (2H, t, pyH), 7.60 (1H, d, pyH), 7.65 (1H, t, pyH). ESI-TOF/MS (in acetonitrile containing a small amount of formic acid): m/z 320 [M + H]⁺.

Synthesis of Modified Ligands Produced by Oxidation Reaction. Me-dpa. A methanol solution (50 mL) of 2-(aminomethyl)pyridine (2.403 g, 22 mmol) was added to a methanol solution (50 mL) of 6-methylpyridine-2-aldehyde (4.845 g, 20 mmol). To the resulting solution was slowly added NaBH₄ (0.832 g, 22 mmol) with stirring at room temperature. After the solution was stirred for a day, HCl was added until the pH of the solution became 1 to decompose an excess of NaBH₄. An aqueous solution of NaOH was added to make the solution basic, and the solution was concentrated under reduced pressure to remove methanol. The resulting solution was extracted with Et₂O (3 × 100 mL). The combined extracts were dried over Na₂SO₄, and Et₂O was removed by evaporation under reduced pressure to give a yellow oil of Me-dpa. ¹H NMR (CDCl₃, 300 MHz): δ 2.54 (3H, s, CH₃), 3.94 (2H, s, CH₂), 3.99 (2H, s, CH₂), 7.01 (1H, d, pyH), 7.15 (1H, t, pyH), 7.16 (1H, d, pyH), 7.36 (1H, d, pyH), 7.52 (1H, t, pyH), 7.64 (1H, t, pyH), 8.56 (1H, d, pyH). ESI-TOF/MS (in acetonitrile containing a small amount of formic acid): m/z 427 [2M + H]⁺.

Me-tpa-CH₂OH. A CHCl₃ solution (50 mL) of Me-dpa (1.066 g, 5 mmol) was added to an aqueous Na₂CO₃ solution (0.530 g, 5 mmol, 50 mL) of 2-bromomethyl-6-hydroxymethylpyridine (0.940 g, 5 mmol). The mixture was stirred vigorously for 3 days. The resulting solution was extracted with CHCl₃ (3 × 50 mL). The combined extracts were dried over Na₂SO₄, and CHCl₃ was removed by evaporation under reduced pressure to give a brown oil of Me-tpa-CH₂OH. ¹H NMR (CDCl₃, 300 MHz): δ 2.53 (3H, s, CH₃), 3.94 (2H, s, CH₂), 3.96 (4H, s, CH₂), 4.73 (2H, s, CH₂-OH), 6.96 (1H, d, pyH), 7.05 (1H, d, pyH), 7.15 (1H, t, pyH), 7.34 (2H, d, pyH), 7.51–7.71 (4H, m, pyH), 8.54 (1H, d, pyH). ESI-TOF/MS (in acetonitrile containing a small amount of formic acid): m/z 335 [M + H]⁺.

Syntheses of Complexes. All of the complexes were prepared under N₂ using Schlenk techniques. [Ni₂(OH)₂(tpa)₂](ClO₄)₂ (**1**^{tpa}-(ClO₄)₂),²⁴ [Ni₂(OH)₂(Me₃-tpa)₂](ClO₄)₂·CH₃COCH₃ (**1**^{Me₃-tpa}-(ClO₄)₂),¹⁷ [Ni₂(O)₂(Me₃-tpa)₂](ClO₄)₂·3H₂O (**2**^{Me₃-tpa}-(ClO₄)₂),¹⁷ [Ni₂(O)₂(Me₂-tpa)₂](ClO₄)₂·3H₂O (**3**^{Me₂-tpa}-(ClO₄)₂),¹⁷ [Ni₂(OH)₂(Me₂-tpa)₂](ClO₄)₂·3H₂O (**1**-(ClO₄)₂),²¹ and [Ni₂(Me-tpa-CH₂OO)₂](ClO₄)₂·H₂O (**5**-(ClO₄)₂)²¹ were prepared according to the literature methods.

Caution: Perchlorate salts are potentially explosive and should be handled with care.

[Ni₂(OH)₂(Me-tpa)₂](ClO₄)₂·H₂O (**1**^{Me-tpa}-(ClO₄)₂). To a mixture of Ni(ClO₄)₂·6H₂O (183 mg, 0.5 mmol) and Me-tpa (152 mg, 0.5 mmol) in methanol (20 mL) was added 1 M *n*-Bu₄NOH in methanol (175 μ L, 0.5 mmol) with stirring. The resulting solution was allowed to stand overnight at 0 °C to afford **1**^{Me-tpa} as blue crystals. Yield: 230 mg (94%). Anal. Calcd for C₃₈H₄₄N₈Cl₂Ni₂O₁₁: C, 46.71; H, 4.54; N, 11.47. Found: C, 46.64; H, 4.52; N, 11.45. IR (KBr, cm⁻¹): 3631, 1604, 1577, 1484, 1457, 1351, 1091, 765, 624. ESI-TOF/MS (in acetonitrile): m/z 379 [M]²⁺.

(22) Nagao, H.; Komeda, N.; Mukaida, M.; Suzuki, M.; Tanaka, K. *Inorg. Chem.* **1996**, *35*, 6809.

(23) Sitter, A. J.; Terner J. J. *Labelled Compd. Radiopharm.* **1985**, *22*, 461.

(24) Ito, M.; Sakai, K.; Tsubomura, T.; Takita, Y. *Bull. Chem. Soc. Jpn.* **1999**, *72*, 239.

[Ni₂(O)₂(Me₂-tpa)₂](ClO₄)₂ (2-(ClO₄)₂). Because complex **2** could not be obtained by the reaction of **1** with H₂O₂ (vide infra), **2** was prepared by disproportionation of **3** as follows. **3** (ca. 100 mg) was dissolved in 5 mL of acetone at -40 °C. The resulting solution was allowed to stand for a few days, during which its color changed from dark green to dark brown, and it afforded a brown powder. ESI-TOF/MS spectra of the samples always showed two signals at *m/z* (relative intensity (%)): 392 (100) and 400 (~30), attributable to **2** and [Ni₂(OH)(Me₂-tpa)(Me-tpa-CH₂OO)]²⁺ (**4**), respectively (see the Supporting Information, Figure S1). Repeated purification by addition of ether into an acetone solution of **2** did not improve the purity. UV-vis (λ_{max} (nm) (ϵ (M⁻¹ cm⁻¹)) in acetonitrile at -40 °C): 376 (~6000). ESI-TOF/MS (in acetonitrile at -40 °C): *m/z* 392 [M]²⁺. Because the complex is unstable at room temperature, elemental analysis was not carried out.

[Ni₂(O)₂(Me₂-tpa)₂](BPh₄)₂ (2-(BPh₄)₂). Complex **2**-(ClO₄)₂ (ca. 100 mg) was dissolved in a small amount of a 1:1 acetone:acetonitrile mixture at -40 °C, to which was added NaBPh₄ (68 mg). The resulting solution was allowed to stand for a few days at -70 °C, giving dark brown crystals suitable for X-ray crystallography.

[Ni₂(O)₂(Me₂-tpa)₂](ClO₄)₂ (3-(ClO₄)₂). Aqueous 30% H₂O₂ (220 μ L, 2 mmol) was added to a methanol solution (15 mL) containing Ni(NO₃)₂·6H₂O (0.058 g, 0.2 mmol), Me₂-tpa (0.064 g, 0.2 mmol), and 1 M *n*-Bu₄NOH in methanol (140 μ L, 0.4 mmol) at -40 °C, producing a dark green solution, to which was added a solution of NaClO₄·H₂O (0.056 g, 0.4 mmol) in methanol (1 mL). The resulting solution was left for a few days at -70 °C, giving **3** as dark green crystals. UV-vis (λ_{max} (nm) (ϵ (M⁻¹ cm⁻¹)) in acetonitrile at -40 °C): 335 (~11 000). ESI-TOF/MS (in acetonitrile at -40 °C; a monomeric species was detected): *m/z* 408 [M]⁺ (*m/z* 412 for ¹⁸O). Because the complex is unstable at room temperature, elemental analysis was not carried out.

[Ni₂(O)₂(Me₂-tpa)₂](BPh₄)₂·4CH₃COCH₃ (3-(BPh₄)₂·4CH₃-COCH₃). Complex **3**-(ClO₄)₂ (ca. 100 mg) was dissolved in a small amount of a 1:1 acetone:acetonitrile mixture at -40 °C, to which was added NaBPh₄ (68 mg). The resulting solution was allowed to stand for a few days at -70 °C, giving dark green crystals suitable for X-ray crystallography.

[Ni₂(OH)(Me₂-tpa)(Me-tpa-CH₂OO)](BPh₄)₂·4CH₃CN (4-(BPh₄)₂·4CH₃CN). To an acetonitrile solution (15 mL) of **3** (ca. 100 mg) was added a solution of NaBPh₄ in acetonitrile (1 mL) at -40 °C. The mixture was allowed to stand for several days at -20 °C, producing **4** as pink-brown crystals suitable for X-ray crystallography. ESI-TOF/MS (in acetonitrile): *m/z* 400 [M]²⁺. Because the complex is unstable at room temperature, elemental analysis was not carried out.

Physical Measurements. Electronic spectra were measured with a Simadzu diode array spectrometer Multispec-1500 or an Otsuka Electronics MCPD-2000 photodiode array spectrometer with an Otsuka Electronics optical fiber attachment. The temperatures were controlled with a Unisoku thermostated cell holder for the former instrument and with a EYELA low-temperature pairstirrer PSL-1800 for the latter one. The reflectance spectra were obtained with an Otsuka Electronics MCPD-2000 photodiode array spectrometer with an Otsuka Electronics optical fiber attachment. The crystalline samples were finely ground and spread on a white filter paper attached to a handmade cold copper plate immersed inside a liquid N₂ Dewar vessel at ca. -80 °C. Infrared spectra were obtained by the KBr disk method with a HORIBA FT-200 spectrophotometer.

¹H NMR spectra were measured with a JEOL JNM-LM300 or JNM-LM400 instrument using tetramethylsilane (TMS) or sodium 2,2-dimethyl-2-silapentane-5-sulfonate (NaDSS) as an internal

standard. For quantitative analyses of ligand recovery experiments, we used NaDSS and 2,6-dimethyl-1,4-benzoquinone as internal standards. ESI-TOF/MS spectra were measured with a Micromass LCT spectrometer. Accurate masses (in *m/z*) are referenced to tetra-*n*-decylammonium ion (*m/z* = 578.6604) or tetrabutylammonium ion (*m/z* = 242.2848) as an internal standard.

The EPR spectra were measured with a JEOL X-band spectrometer (JES-RE1XE) using an attached VT apparatus and were recorded under nonsaturating microwave power conditions. The magnitude of the modulation was chosen to optimize the resolution and the signal-to-noise ratio of the observed spectra. The *g* values were calibrated with a Mn²⁺ marker.

Resonance Raman spectra were obtained with a liquid-N₂-cooled CCD detector (LN/CCD-1100-PB, Roper Scientific) attached to a 1 m single polychromator (model MC-100dg, Ritsu Oyo Kogaku). The 406.7 nm line of a Kr⁺ laser (model 2060, Spectra Physics) was used as an exciting source. The laser powers used were ca. 10 mW at the sample point. All measurements were carried out with a spinning cell (1000 rpm) at ca. -40 to ca. -80 °C. Raman shifts were calibrated with indene, and the accuracy of the peak positions of the Raman bands was ± 1 cm⁻¹.

The cyclic voltammetry (CV) measurements were performed on a BAS 100B/W electrochemical analyzer in anhydrous acetonitrile containing 0.1 M *n*-Bu₄NClO₄ as the supporting electrolyte. A Pt working electrode was polished with an alumina (0.06 μ m) paste and then rinsed with acetonitrile before use. The counter electrode was a Pt wire. A Ag/Ag⁺ couple was used as a reference electrode, and the potentials were determined using the ferrocene/ferrocenium (Fc/Fc⁺) couple as a reference. Measurements were carried out at 20 and -40 °C under N₂.

The XAFS measurements have been performed at BL01B1 at SPring-8 (Hyogo, Japan), which operates at 8 GeV with a current of 100 mA, using a Si(111) double-crystal monochromator and Rh-coated mirrors (Proposal J05A01B1-0502N). The energy calibration was made by nickel foil, as given in Figure S2 of the Supporting Information. Solid samples were diluted with BN powder (~30%) and pressed into pellets (7 mm diameter, ~1 mm thickness) and then measured in transmission mode. The solution samples were introduced into a 2 mm thick cell with Kapton windows and cooled to 100 K. The XAFS spectra of powdery samples and solution samples were taken in transmission mode. The obtained XAFS spectra were analyzed by using the UWXAFS program.²⁵ After background subtraction by the AUTOBK program,²⁶ the Fourier transformation for the *k*³-weighted EXAFS oscillation was performed, and the structural parameters were determined by a curve-fitting procedure in the R space by using the FEFFIT program involving multiple scattering effects.²⁷

$$\chi(k) = \sum_j S_0^2 N_j \frac{F_j(k)}{kR_j^2} \sin(2R_jk + \delta_j(k)) \exp\left(-2k^2\sigma_j^2 - \frac{2R_j}{\lambda_j(k)}\right)$$

where $F_j(k)$ is the backscattering amplitude from each of the N_j scatterers at distance R_j from the X-ray absorbing atom, $\delta_j(k)$ is the central-atom phase shift, σ_j^2 is the mean-square fluctuation in R_j , $\lambda_j(k)$ is the mean free path of the photoelectron, and S_0^2 is the overall amplitude reduction factor. The values of $F_j(k)$, $\delta_j(k)$, and $\lambda_j(k)$ were generated by the FEFF code. The high-precision static

(25) Stern, E. A.; Newville, M.; Ravel, B.; Yacoby, Y.; Haskel, D. *Physica B* **1995**, *208*, 117.

(26) Newville, M.; Livins, P.; Yacoby, Y.; Stern, E. A.; Rehr, J. J. *Phys. Rev. B* **1993**, *47*, 14126.

(27) Ankudinov, A. L.; Ravel, B.; Rehr, J. J.; Conradson, S. D. *Phys. Rev. B* **1998**, *58*, 7565.

EXAFS data were analyzed in the range of $0.8 \text{ \AA} \leq R \leq 6.0 \text{ \AA}$ by considering all the single- and multiple-scattering contributions.

The curve-fitting analyses (R and DW) of Ni–O and Ni–N were carried out assuming that the CN values of the Ni–O and Ni–N are 2 and 4, respectively, on the basis of the X-ray analysis. The structural parameters of Ni \cdots Ni were obtained, including thus-obtained Ni–N and Ni–O structural parameters.

Isolation and Identification of Modified Ligands by Ligand Recovery. Thermal Decomposition of 2. Thermal decomposition was performed under both N₂ and O₂. Typically, **2** (ca. 100 mg) was dissolved into 20 mL of acetonitrile at $-40 \text{ }^\circ\text{C}$. The resulting solution was warmed to room temperature under N₂ and allowed to stand for a week to produce a pale-yellow solution (a yellow solution under O₂). The volume of the resulting solution was adjusted to 50 mL with acetone. Because it was difficult to weigh the amount of **2** because of its thermal instability, a portion (10 mL) was taken up and the concentration of the nickel ion was determined by atomic absorption spectrophotometry. Quantitative analyses for Me₂-tpa, (Me-tpa-CH₂)₂, Me-tpa-CH₂OH, Me-tpa-CHO, Me-tpa-COO⁻, and N-dealkylated ligand were as follows. A portion (10 mL) from the above remaining solution was taken up, and the solvent was removed under reduced pressure to give a brown oil. For analyses of Me₂-tpa, (Me-tpa-CH₂)₂, Me-tpa-CH₂OH, Me-tpa-CHO, and N-dealkylated ligand, concentrated Na₄-EDTA·4H₂O (15 mL) was added to the above brown oil, and the ligand and its reaction products except for Me-tpa-COO⁻ were then extracted into chloroform (5 × 20 mL). The combined extract was dried over Na₂SO₄ and the solvent was removed under reduced pressure to give a brown oil. Me₂-tpa, (Me-tpa-CH₂)₂, Me-tpa-CH₂OH, Me-tpa-CHO (trace), and N-dealkylated ligand (Me-dpa = (6-methyl-2-pyridylmethyl)(2-pyridylmethyl)amine) were identified by comparison of ¹H NMR and ESI-TOF/MS of the authentic samples except for Me-tpa-CHO, and their amounts were determined by ¹H NMR by the addition of 2,6-dimethyl-*p*-benzoquinone as an internal standard. For analysis of Me-tpa-COO⁻, we dissolved the brown oil obtained after evaporation of the solvent from a decomposed solution in *d*₇-DMF (0.3 mL), to which was added a solution of NaCN (30 mg) in D₂O (0.2 mL). Me-tpa-COO⁻ was identified by comparison of ¹H NMR and ESI-TOF/MS of the authentic sample obtained from [Ni(Me-tpa-COO⁻)H₂O·ClO₄].²¹ The amount of Me-tpa-COO⁻ was determined by ¹H NMR by the addition of a known amount of sodium 2,2-dimethyl-2-silapentane-5-sulfonate (NaDSS) as an internal standard.

Yields of (Me-tpa-CH₂)₂, N-dealkylated ligand, Me-tpa-COO⁻, Me-tpa-CH₂OH, and Me-tpa-CHO under N₂ were 26, 18, 13, and 6%, and a trace amount, respectively, on the basis of a total amount of Me₂-tpa ligand. Hereafter, yields are reported on the basis of a total amount of Me₂-tpa ligand unless otherwise stated. Under O₂, no (Me-tpa-CH₂)₂ was detected. Yields of Me-tpa-COO⁻, N-dealkylated ligand, and Me-tpa-CH₂OH were 38, 18, and 12%, respectively.

(Me-tpa-CH₂)₂ was isolated as an oil by thin-layer chromatography and identified by ¹H NMR and ESI-TOF/MS. ¹H NMR (CDCl₃, 300 MHz): δ 2.52 (6H, s, CH₃), 3.18 (4H, s, CH₂CH₂), 3.85 (8H, s, CH₂), 3.88 (4H, s, CH₂), 6.95–7.67 (18H, m, pyH), 8.52 (2H, d, pyH). ESI-TOF/MS: m/z 318 [M + 2H]²⁺ and m/z 635 [M + H]⁺.

Identifications of the modified ligand Me-tpa-CH₂OH and the N-dealkylated ligand were carried out by ¹H NMR and ESI-TOF/MS. ¹H NMR for Me-tpa-CH₂OH (CDCl₃, 300 MHz): δ 2.53 (3H, s, CH₃), 3.94 (2H, s, CH₂), 3.96 (4H, s, CH₂), 4.73 (2H, s, CH₂-OH), 6.96 (1H, d, pyH), 7.05 (1H, d, pyH), 7.15 (1H, t, pyH), 7.34 (2H, d, pyH), 7.51–7.71 (4H, m, pyH), 8.54 (1H, d, pyH). ESI-

TOF/MS for Me-tpa-CH₂OH: m/z 335 [M + H]⁺. ¹H NMR for the N-dealkylated ligand (CDCl₃, 300 MHz): δ 2.54 (3H, s, CH₃), 3.94 (2H, s, CH₂), 3.99 (2H, s, CH₂), 7.01 (1H, d, pyH), 7.15 (1H, t, pyH), 7.16 (1H, d, pyH), 7.36 (1H, d, pyH), 7.52 (1H, t, pyH), 7.64 (1H, t, pyH), 8.56 (1H, d, pyH). ESI-TOF/MS for the N-dealkylated ligand: m/z 427 [2M + H]⁺.

Thermal Decomposition of 3. The ligand-recovery experiment for **3** was also performed in the same manner as that for **2**. Yields of (Me-tpa-CH₂)₂, Me-tpa-CH₂OH, Me-tpa-CHO, Me-tpa-COO⁻, and N-dealkylated ligand under N₂ were 10, 18, 4, 18, and 20%, respectively. Yields of Me-tpa-CH₂OH, Me-tpa-COO⁻, and N-dealkylated ligand under O₂ were 11, 44, and 18%, respectively. No coupling dimer was detected.

X-ray Crystallography. Single crystals of **2**·(BPh₄)₂, **3**·(BPh₄)₂·4CH₃COCH₃, and **4**·(BPh₄)₂·4CH₃CN were picked from solutions by a nylon loop (Hampton Research Co.) on a handmade copper plate mounted inside a liquid N₂ Dewar vessel at ca. $-80 \text{ }^\circ\text{C}$ and mounted on a goniometer head in a N₂ cryostream.

Data collections were carried out on a Rigaku/MSC Mercury diffractometer with graphite monochromated Mo K α radiation ($\lambda = 0.71070 \text{ \AA}$). The data were collected at $-150 \pm 1 \text{ }^\circ\text{C}$ to a maximum 2θ value of 61.0° for **2**·(BPh₄)₂ and **3**·(BPh₄)₂·4CH₃COCH₃ and 55.0° for **4**·(BPh₄)₂·4CH₃CN. A total of 720 oscillation images were collected. A first sweep of data was done using ω scans from -80.0 to 100.0° in 0.50° steps, at $\chi = 45.0^\circ$ and $\phi = 0.0^\circ$. A second sweep of data was made using ω scans from -80.0 to 100.0° in a 0.50° step, at $\chi = 45.0^\circ$ and $\phi = 90.0^\circ$. Crystal-to-detector distances were 35 mm, and detector swing angles were 10° . Exposure rates were 30.0, 100.0, and 30.0 s/deg for **2**·(BPh₄)₂, **3**·(BPh₄)₂·4CH₃COCH₃, and **4**·(BPh₄)₂·4CH₃CN, respectively. The data were corrected for Lorentz and polarization effects. Empirical absorption corrections were applied.

The structures were solved by a direct method (SIR92)²⁸ and expanded using a Fourier technique.²⁹ The structures were refined by a full-matrix least-squares method by using the teXsan³⁰ crystallographic software package (Molecular Structure Corporation). The structure refinements were carried out by the observations ($I > 3.0\sigma(I)$). Non-hydrogen atoms, except for those of solvent molecules in **4**·(BPh₄)₂·4CH₃CN, were refined with anisotropic displacement parameters. Hydrogen atoms were positioned at the calculated positions (0.95 Å). They were included, but not refined, in the final least-squares cycles. Crystallographic data are summarized in Table 1. ORTEP views (50% probability level) of the complex cations of **2**·(BPh₄)₂, **3**·(BPh₄)₂·4CH₃COCH₃, and **4**·(BPh₄)₂·4CH₃CN with a full numbering scheme of atoms are shown in Figure S3, S4, and S5, respectively, of the Supporting Information. Tables of the final atomic coordinates, thermal parameters, and full bond distances and angles are given in the CIF data in the Supporting Information.

[Ni₂(O)₂(Me₂-tpa)₂](BPh₄)₂ (2-(BPh₄)₂). Half of a [Ni₂(O)₂(Me₂-tpa)₂]²⁺ ion and one BPh₄⁻ molecule are contained in an asymmetric unit. The final R (R_w) values were 0.056 (0.094).

[Ni₂(O)₂(Me₂-tpa)₂](BPh₄)₂·4CH₃COCH₃ (3-(BPh₄)₂·4CH₃COCH₃). Half of a [Ni₂(O)₂(Me₂-tpa)₂]²⁺ ion, one BPh₄⁻ molecule,

(28) Altomare, A.; Casciarano, G.; Giacovazzo, C.; Guagliardi, A.; Burla, M. C.; Polidori, G.; Camalli, M. *SIR-92*; *J. Appl. Crystallogr.* **1994**, *27*, 435.

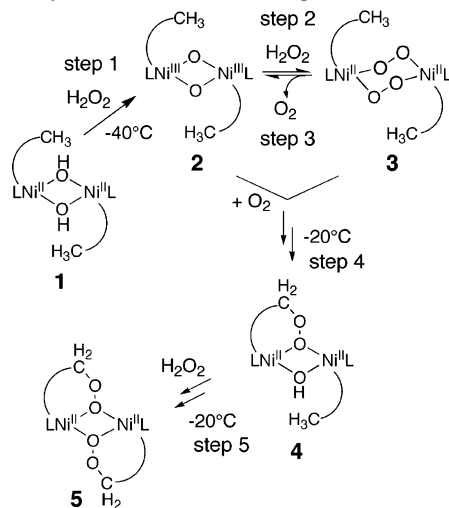
(29) Beurskens, P. T.; Admiraal, G.; Beurskens, G.; Bosman, W. P.; de Gelder, R.; Israel, R.; Smits, J. M. M. *The DIRDIF-94 Program System*; Technical Report of the Crystallography Laboratory; University of Nijmegen: Nijmegen, The Netherlands, 1994.

(30) *teXsan: Crystal Structure Analysis Package*; Molecular Structure Corporation: The Woodlands, TX, 1985 and 1992.

Table 1. Crystallographic Data for **2**-(BPh₄)₂, **3**-(BPh₄)₂·4CH₃COCH₃, and **4**-(BPh₄)₂·4CH₃CN

	2 -(BPh ₄) ₂	3 -(BPh ₄) ₂ ·4CH ₃ COCH ₃	4 -(BPh ₄) ₂ ·4CH ₃ CN
formula	C ₈₈ H ₈₄ N ₈ B ₂ O ₂ Ni ₂	C ₁₀₀ H ₁₀₈ N ₈ B ₂ O ₈ Ni ₂	C ₉₆ H ₉₆ N ₁₂ B ₂ O ₃ Ni ₂
<i>T</i> (°C)	−150	−150	−150
mol wt	1424.70	1689.02	1604.91
cryst syst	triclinic	monoclinic	triclinic
space group	<i>P</i> $\bar{1}$	<i>P</i> 2 ₁ / <i>n</i>	<i>P</i> $\bar{1}$
<i>a</i> (Å)	11.620(2)	16.483(6)	13.729(2)
<i>b</i> (Å)	13.213(2)	14.225(5)	14.489(2)
<i>c</i> (Å)	14.053(1)	18.895(9)	23.018(3)
α (deg)	67.46(1)	90	83.64(1)
β (deg)	66.03(1)	94.153(10)	76.888(10)
γ (deg)	88.76(2)	90	72.95(1)
<i>V</i> (Å ³)	1797.8(5)	4419(3)	4258.5(11)
<i>Z</i>	1	2	2
2 θ _{max}	61.0	61.0	55.0
<i>F</i> (000)	750.00	1740.00	1692.00
<i>D</i> _{calcd} (g/cm ³)	1.316	1.251	1.251
abs coeff (cm ^{−1})	5.81	4.88	5.00
no. of reflns collected	21620	50675	28068
no. of indep reflns	8854	11552	18797
no. of refined params	460	541	988
GOF indication	1.515	1.320	1.565
largest peak/hole (e Å ^{−3})	0.66/−0.47	0.90/−0.41	0.97/−0.38
<i>R</i> ^a	0.056	0.061	0.067
<i>R</i> _w ^b	0.094	0.087	0.094

^a $R = \sum[|F_o| - |F_c|]/\sum|F_o|$ ($I \geq 3.0\sigma(I)$). ^b $R_w = [\sum w(|F_o| - |F_c|)^2/\sum w|F_o|^2]^{1/2}$; $w = 1/[\sigma^2(F_o) + p^2|F_o|^2/4]$ ($p = 0.085$ for **2**-(BPh₄)₂, $p = 0.092$ for **3**-(BPh₄)₂·4CH₃COCH₃, and $p = 0.075$ for **4**-(BPh₄)₂·4CH₃CN).

Scheme 1. Synthetic Procedures for Complexes

and two acetone molecules are contained in an asymmetric unit. The final *R* (*R*_w) values were 0.061 (0.087).

[Ni₂(OH)(Me₂-tpa)(Me-tpa-CH₂OO)](BPh₄)₂·4CH₃CN (**4**-(BPh₄)₂·4CH₃CN). The asymmetric unit consists of a [Ni₂(OH)(Me₂-tpa)(Me-tpa-CH₂OO)]²⁺ ion, two BPh₄[−] ions, and four solvent molecules, which were solved by a disordered model with isotropic thermal parameters. The final *R* (*R*_w) values were 0.067 (0.094).

Results

Synthesis of Complexes. Synthetic procedures for the sequential reaction intermediates are summarized in Scheme 1. The reaction of [Ni₂(OH)₂(Me₂-tpa)₂]²⁺ (**1**) with excess H₂O₂ in methanol at −40 °C caused a color change from sky blue to dark green. From the reaction mixture, we

isolated a bis(μ-superoxo)nickel(II) complex ([Ni₂(O₂)₂-(Me₂-tpa)₂]²⁺ (**3**)) at a temperature below −70 °C. The formation of **3** suggests the presence of a bis(μ-oxo)nickel(III) species as a reaction intermediate (vide infra), which can oxidize peroxide to superoxide to generate **3** through step 1 to step 2 in Scheme 1, as found for the Me₃-tpa system.¹⁷ Unlike in the Me₃-tpa system, however, the ESI-TOF/MS spectrum of the reaction solution did not show any evidence for the existence of the bis(μ-oxo)nickel(III) complex ([Ni₂(O)₂(Me₂-tpa)₂]²⁺ (**2**)) under the experimental conditions, even though a small amount of H₂O₂ (0.2 equiv) was used at −80 °C. The result suggests that **2** is extremely reactive with H₂O₂ compared to [Ni₂(O)₂(Me₃-tpa)₂]²⁺ (**2**^{Me₃-tpa}). However, the reaction of **2** (vide infra) with H₂O₂ produced **3**, which was confirmed by ESI-TOF/MS. Such a high reactivity of **2** toward H₂O₂ may be attributable to the structural feature of **2** (vide infra). Thus, H₂O₂ prevents the detection and isolation of **2**. However, **2** was obtained by disproportionation of the superoxo ligands in **3** in acetonitrile at −40 °C, which was confirmed by ESI-TOF/MS (Figure 1a), although, as mentioned in the Experimental Section, the reaction always gave some amount of [Ni₂(OH)(Me₂-tpa)(Me-tpa-CH₂OO)]²⁺ (**4**) as an impurity. In contrast, **2**^{Me₃-tpa} was not obtained by disproportionation of [Ni₂(O)₂-(Me₃-tpa)₂]²⁺ (**3**^{Me₃-tpa}), because **2**^{Me₃-tpa} is not stable and decomposes via oxidation of the Me₃-tpa ligand under similar reaction conditions.¹⁷ Complex **2** is substantially stable compared to **2**^{Me₃-tpa} at −40 °C (vide infra).

It is noted that thermal decomposition of **3** at temperatures above −20 °C gave a ligand-based alkylperoxo complex [Ni₂(OH)(Me₂-tpa)(Me-tpa-CH₂OO)]²⁺ (**4**) via **2** under O₂, as shown in Figure 1b. Complex **4** is in equilibrium between [Ni₂(OH)₂(Me₂-tpa)₂]²⁺ (**1**) and [Ni₂(Me-tpa-CH₂OO)₂]²⁺ (**5**), although the equilibrium (eq 1) lies to the left. Complex **5**

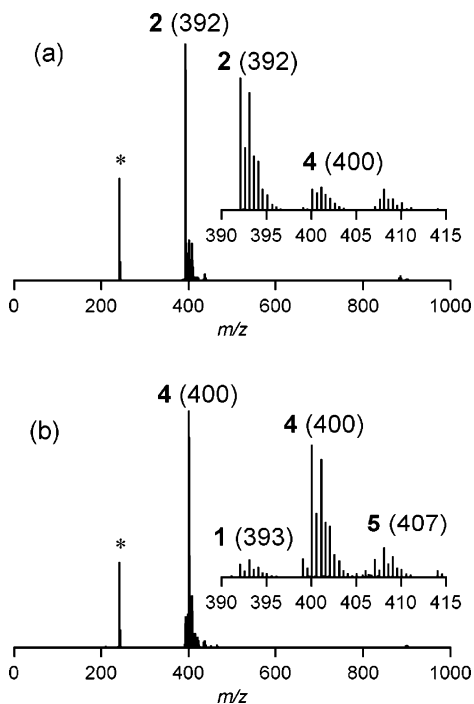
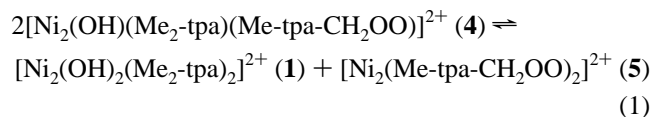


Figure 1. ESI-TOF/MS spectra of (a) **2** (m/z 392) generated by standing **3** for several hours at -40 °C and (b) **4** (m/z 400) generated by warming **3** at -20 °C for several hours. The asterisk (*) is an internal standard signal $[(\text{CH}_3(\text{CH}_2)_3)_4\text{N}]^+$ (m/z 242.848).

can be prepared by the reaction of **1** with excess H_2O_2 at -20 °C, as reported previously.²¹



Structure Description of 2, 3, and 4. The sequential reaction intermediates **2**, **3**, and **4** were successfully characterized by X-ray crystallography. The ORTEP drawings of the complex cations of **2**, **3**, and **4** are shown in Figure 2, and selected bond distances and angles are listed in Table 2. Complex **2** has a centrosymmetric $\text{Ni}^{\text{III}}(\mu\text{-O})_2\text{Ni}^{\text{III}}$ core with N_4 donors of the $\text{Me}_2\text{-tpa}$, where 2-pyridylmethyl sidearms

are in the equatorial positions as found for a corresponding bis(μ -oxo)dicopper(III) complex, $[\text{Cu}_2(\text{O})_2(\text{Me}_2\text{-tpa})_2]^{2+}$ (**2^{Cu}**).^{9f} The average Ni–O and Ni–N bond distances (1.852 and 2.130 Å) and the Ni \cdots Ni separation (2.796(1) Å) of **2** are significantly shorter than those of $[\text{Ni}_2(\text{OH})_2(\text{Me}_2\text{-tpa})_2]^{2+}$ (**1**)²¹ (2.013, 2.182, and 3.029(1) Å, respectively). The average Ni– N_{axial} bond distance (2.285 Å) is substantially longer than the average Ni– $\text{N}_{\text{equatorial}}$ bond distance (1.975 Å). This elongation of the axial bonds is attributable to the Jahn–Teller effect arising from a low-spin d^7 electron configuration. It is also noted that the average Ni– N_{axial} bond distance (2.285 Å) is substantially shorter than that of **2^{Cu}** (2.515 Å).^{9f} The long axial bonds in **2^{Cu}** may be ascribed to a d^8 electron configuration, which tends to adopt a square planar structure. The average Ni–O and Ni–N bond distances and the Ni \cdots Ni separation of **2** are slightly shorter than those in **2^{Me₃-tpa}** (1.871, 2.143, and 2.924(1) Å, respectively). However, the Ni–N2 bond distance (1.942(4) Å) of the in-plane pyridyl group in **2** is significantly shorter than the corresponding bond distance (2.045(9) Å) of the in-plane 6-methylpyridyl group in **2^{Me₃-tpa}**,¹⁷ in the latter of which the 6-methyl group prevents a close approach of the pyridyl group to the nickel atom by steric requirements. The in-plane 6-methylpyridyl groups of **2^{Me₃-tpa}** form a hydrophobic cavity around a $\text{Ni}^{\text{III}}(\mu\text{-O})_2\text{Ni}^{\text{III}}$ core, which has a significant influence on the reactivity with H_2O_2 (vide infra).

Complex **3** has a centrosymmetric $\text{Ni}^{\text{II}}(\mu\text{-OO})_2\text{Ni}^{\text{II}}$ core with $\text{Me}_2\text{-tpa}$ nitrogens, as found for $[\text{Ni}_2(\text{O})_2(\text{Me}_3\text{-tpa})_2]^{2+}$ (**3^{Me₃-tpa}**).¹⁷ The nickel centers in a distorted octahedral structure are linked by two μ -1,2-O–O bridges to form a six-membered ring with chair conformation having a Ni–O–O–Ni torsion angle of 86.8°. The average Ni–O bond distance of **3** (1.947 Å) is significantly longer than that of **2** (1.852 Å) but shorter than that of **1** (2.013 Å). The O–O bond distance of **3** (1.338(3) Å) is comparable to that of **3^{Me₃-tpa}** (1.345(6) Å).

The crystal structure of **4** consists of two Ni(II) centers linked by a hydroxo bridge in one side and an alkylperoxo bridge in the other side, the latter of which is a ligand-based

Table 2. Selected Bond Distances and Angles for **2**-(BPh₄)₂, **3**-(BPh₄)₂·4CH₃COCH₃, and **4**-(BPh₄)₂·4CH₃CN

Bond Distances (Å)							
2-(BPh ₄) ₂		3-(BPh ₄) ₂ ·4CH ₃ COCH ₃		4-(BPh ₄) ₂ ·4CH ₃ CN			
Ni1–O1	1.845(3)	Ni1–O1	1.937(2)	Ni1–O1	1.978(4)	Ni2–O1	2.068(4)
Ni1–O1*	1.858(3)	Ni1–O2*	1.956(2)	Ni1–O3	2.086(6)	Ni2–O3	2.021(5)
Ni1–N1	2.008(4)	Ni1–N1	2.053(3)	Ni1–N1	2.084(4)	Ni2–N5	2.079(4)
Ni1–N2	1.942(4)	Ni1–N2	2.056(3)	Ni1–N2	2.034(5)	Ni2–N6	2.084(5)
Ni1–N3	2.206(4)	Ni1–N3	2.130(3)	Ni1–N3	2.237(5)	Ni2–N7	2.194(5)
Ni1–N4	2.363(4)	Ni1–N4	2.162(3)	Ni1–N4	2.169(5)	Ni2–N8	2.183(5)
Ni1 \cdots Ni1*	2.796(1)	Ni1 \cdots Ni1*	3.838(1)	Ni1 \cdots Ni2	3.154(1)	O1–O2	1.462(6)
		O1–O2	1.338(3)				
Bond Angles (deg)							
2-(BPh ₄) ₂		3-(BPh ₄) ₂ ·4CH ₃ COCH ₃		4-(BPh ₄) ₂ ·4CH ₃ CN			
Ni1–O1–Ni1*	98.1(1)	O1–Ni1–O2*	82.54(10)	Ni1–O1–Ni2			102.4(2)
O1–Ni1–O1*	81.9(1)	Ni1–O1–O2	113.6(2)	Ni1–O3–Ni2			100.4(2)
		Ni1–O2*–O1*	116.1(2)	O1–Ni1–O3			78.6(2)
				O1–Ni2–O3			78.1(2)
				Ni1–O1–O2			110.6(3)
				Ni2–O1–O2			124.3(3)

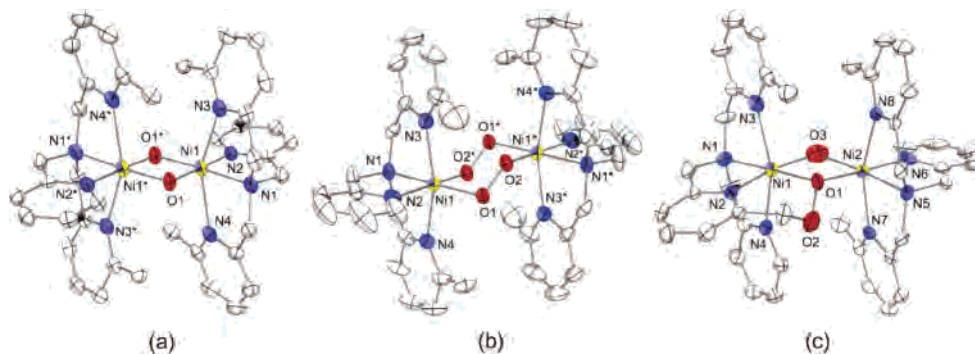


Figure 2. ORTEP views (50% probability level) of (a) $[\text{Ni}_2(\text{O})_2(\text{Me}_2\text{-tpa})_2]^{2+}$ (**2**), (b) $[\text{Ni}_2(\text{O}_2)_2(\text{Me}_2\text{-tpa})_2]^{2+}$ (**3**), and (c) $[\text{Ni}_2(\text{OH})(\text{Me}_2\text{-tpa})(\text{Me-tpa-CH}_2\text{OO})]^{2+}$ (**4**). Hydrogen atoms are omitted for clarity.

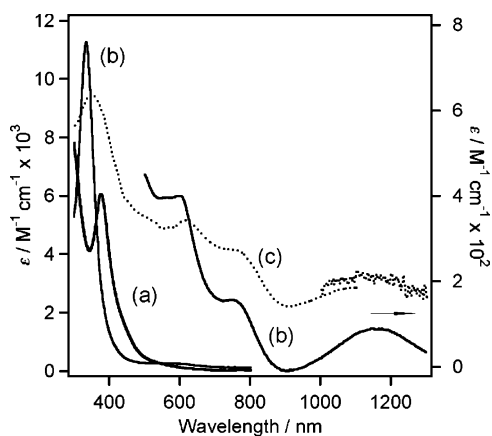


Figure 3. Absorption spectra of (a) **2** in acetonitrile at $-40\text{ }^\circ\text{C}$ and (b) **3** in acetonitrile at $-40\text{ }^\circ\text{C}$. Reflectance spectrum of (c) a powdered sample of **3** at ca. $-80\text{ }^\circ\text{C}$ (intensity scale is arbitrary).

alkylperoxide derived from the oxidation of one of the methyl groups in the $\text{Me}_2\text{-tpa}$ ligand. The O–O bond distance of $1.462(6)\text{ \AA}$ in **4** is comparable to that of **5** ($1.458(4)\text{ \AA}$)²¹ and in the range of those for transition metal–alkylperoxo complexes ($1.36\text{--}1.52\text{ \AA}$).³¹

Spectroscopic Characterization of 2 and 3. The electronic spectrum of $[\text{Ni}_2(\text{O})_2(\text{Me}_2\text{-tpa})_2]^{2+}$ (**2**) shows an intense band at 376 nm ($\epsilon \approx 6000\text{ M}^{-1}\text{ cm}^{-1}$) in acetonitrile at $-40\text{ }^\circ\text{C}$ (Figure 3a), which is similar to that of $2^{\text{Me}_3\text{-tpa}}$ ($\lambda_{\text{max}} = 394\text{ nm}$, $\epsilon \approx 4000\text{ M}^{-1}\text{ cm}^{-1}$).¹⁷ Such intense absorption bands have also been observed for five-coordinate bis(μ -oxo)dinickel(III) complexes containing tridentate N-donor ligands ($\lambda_{\text{max}} = 405\text{--}414\text{ nm}$).^{15,16} These bands have been assigned to the $\text{O}^{2-}\text{-to-Ni(III)}$ charge-transfer transition (LMCT: $(\sigma_g + d_{x^2-y^2}(+)) \rightarrow (d_{xy}(-) + \sigma_u^*)$) on the basis of theoretical calculations.²⁰ There is a trend in CT transition energies; CT transition energies of the six-coordinate complexes (**2** and $2^{\text{Me}_3\text{-tpa}}$) are higher than those of the five-coordinate complexes, such as $[\text{Ni}_2(\text{O})_2(\text{Tp}^{\text{Me}_3})_2]$ ($\lambda_{\text{max}} = 410\text{ nm}$, $\epsilon = 4200\text{ M}^{-1}\text{ cm}^{-1}$).¹⁵ A similar trend was also

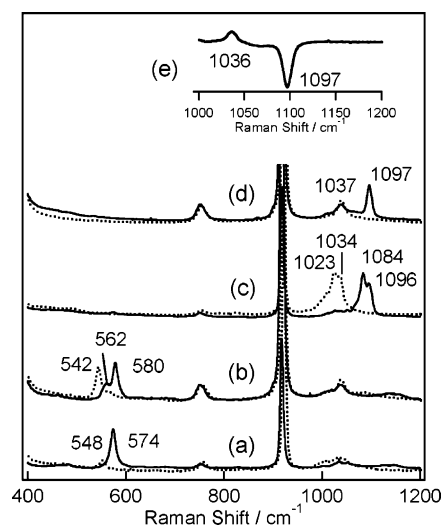


Figure 4. Resonance Raman spectra of (a) **2** in acetonitrile (ca. 1 mM) generated by the reaction of **1** with 0.5 equiv of $\text{H}_2^{16}\text{O}_2$ (solid line) and $\text{H}_2^{18}\text{O}_2$ (dotted line) at $-40\text{ }^\circ\text{C}$ by standing for ca. 10 h ; (b) $2^{\text{Me}_3\text{-tpa}}$ in acetonitrile at $-40\text{ }^\circ\text{C}$ prepared by the reaction of $1^{\text{Me}_3\text{-tpa}}$ with 1 equiv of $\text{H}_2^{16}\text{O}_2$ (solid line) and $\text{H}_2^{18}\text{O}_2$ (dotted line); (c) **3** in acetonitrile (ca. 1 mM) at $-40\text{ }^\circ\text{C}$ prepared by the reaction of **1** with excess of $\text{H}_2^{16}\text{O}_2$ (solid line) and $\text{H}_2^{18}\text{O}_2$ (dotted line); and (d) $3^{\text{Me}_3\text{-tpa}}$ in acetonitrile (ca. 1 mM) at $-40\text{ }^\circ\text{C}$ prepared by the reaction of $1^{\text{Me}_3\text{-tpa}}$ with 5 equiv of $\text{H}_2^{16}\text{O}_2$ (solid line) and $\text{H}_2^{18}\text{O}_2$ (dotted line) obtained with a 406.7 nm laser excitation. Inset (e) is a difference spectrum of $3^{\text{Me}_3\text{-tpa}}$ prepared from $\text{H}_2^{16}\text{O}_2$ and $\text{H}_2^{18}\text{O}_2$.

observed for the corresponding copper complexes.^{9f,i} This may be ascribed to an increase in d orbital energy because of the coordination number increase from five to six (diminishing the Lewis acidity of Ni(III) centers). In addition, the CT transition energy of **2** is higher than that of $2^{\text{Me}_3\text{-tpa}}$.¹⁷ This is also due to a stronger electron donation of $\text{Me}_2\text{-tpa}$, which increases d orbital energy compared to that of $\text{Me}_3\text{-tpa}$. This is supported by the shorter Ni–N2 bond distance ($1.942(4)\text{ \AA}$) of the in-plane pyridyl group in **2** relative to the corresponding Ni–N2 bond distance ($2.045(9)\text{ \AA}$) of the in-plane 6-methylpyridyl group in $2^{\text{Me}_3\text{-tpa}}$.

The resonance Raman spectra ($\lambda_{\text{ex}} = 406.7\text{ nm}$, $T = -40\text{ }^\circ\text{C}$) of **2** and $2^{\text{Me}_3\text{-tpa}}$ in acetonitrile show isotope-sensitive bands at 574 cm^{-1} ($^{16-18}\Delta = 26\text{ cm}^{-1}$) and at 562 and 580 cm^{-1} (Fermi doublet centered at 571 cm^{-1} ; $^{16-18}\Delta = 29\text{ cm}^{-1}$), respectively, as shown in panels a and b of Figure 4. They are characteristic of those of the bis(μ -oxo)dinickel(III) and bis(μ -oxo)dicopper(III) complexes.^{4b,13,16} These values are lower than those of bis(μ -oxo)dinickel(III) complexes with tridentate nitrogen ligands ($599\text{--}612\text{ cm}^{-1}$),¹⁶

(31) (a) Kitajima, N.; Katayama, T.; Fujisawa, K.; Iwata, Y.; Moro-oka, Y. *J. Am. Chem. Soc.* **1993**, *115*, 7872. (b) Komatsuzaki, H.; Sakamoto, N.; Satoh, M.; Hikichi, S.; Akita, M.; Moro-oka, Y. *Inorg. Chem.* **1998**, *37*, 6554. (c) Hikichi, S.; Komatsuzaki, H.; Akita, M.; Moro-oka, Y. *J. Am. Chem. Soc.* **1998**, *120*, 4699. (d) Bonchio, M.; Calloni, S.; Furia, F. D.; Licini, G.; Modena, G.; Moro, S.; Nugent, W. A. *J. Am. Chem. Soc.* **1997**, *119*, 6935. (e) Chavez, F. A.; Mascharak, P. K. *Acc. Chem. Res.* **2000**, *33*, 539. (f) Chen, P.; Fujisawa, K.; Solomon, E. I. *J. Am. Chem. Soc.* **2000**, *122*, 10177. (g) Kujime, M.; Hikichi, S.; Akita, M. *Chem. Lett.* **2003**, *32*, 486.

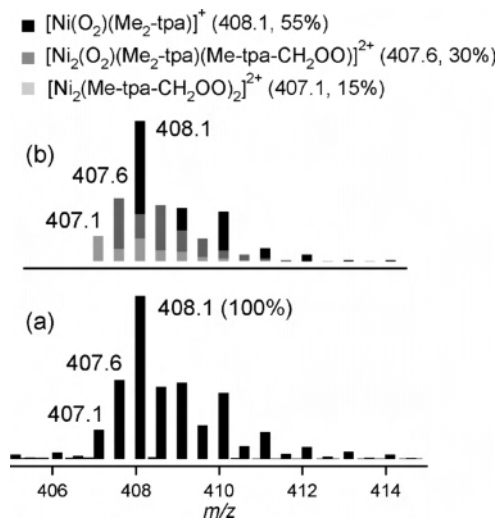


Figure 5. ESI-TOF/MS spectrum of (a) a crystalline sample of **3** in acetonitrile at $-40\text{ }^{\circ}\text{C}$ and (b) a simulated spectrum consisting of $[\text{Ni}(\text{O}_2)(\text{Me}_2\text{-tpa})]^+$ (m/z 408.1), $[\text{Ni}_2(\text{O}_2)(\text{Me}_2\text{-tpa})(\text{Me-tpa-CH}_2\text{OO})]^{2+}$ (m/z 407.6), and $[\text{Ni}_2(\text{Me-tpa-CH}_2\text{OO})_2]^{2+}$ (m/z 407.1).

suggesting that the Ni–O bonds for six-coordinate complexes **2** and $2^{\text{Me}_3\text{-tpa}}$ are weaker than those of the five-coordinate complexes. The lower frequencies observed for the six-coordinate complexes may be in line with weaker Lewis acidity of metal centers in the six-coordinate complexes compared to that of the five-coordinate complexes.

The resonance Raman spectrum of **3** exhibits isotope-sensitive bands at 1084 and 1096 cm^{-1} (1023 and 1034 cm^{-1} for an ^{18}O -labeled sample), and $3^{\text{Me}_3\text{-tpa}}$ exhibits an isotope-sensitive band at 1096 cm^{-1} (1037 cm^{-1} for an ^{18}O -labeled sample), as shown in panels c and d of Figure 4, the latter of which is in agreement with that of a solid sample of $3^{\text{Me}_3\text{-tpa}}$ (1096 cm^{-1}).¹⁷ Although the origin of the two bands observed for **3** is not known at present, there is a possibility that either they are Fermi doublets or two isomers exist.

The ESI-TOF/MS spectrum of a crystalline sample of **3** in acetone at $-40\text{ }^{\circ}\text{C}$ showed a signal at $m/z = 408$ ($I = 100\%$) and a signal at $m/z = 412$ ($I = 100\%$) for an ^{18}O -labeled sample with a complex isotope pattern (Figure 5a), as reported previously.²¹ Analysis of the isotope patterns suggested the presence of a monomeric superoxonickel(II) species, $[\text{Ni}(\text{O}_2)(\text{Me}_2\text{-tpa})]^+$ (m/z 408.10 ($I = 100\%$)), a (μ -superoxo)(μ -alkylperoxo)dinickel(II) species, $[\text{Ni}_2(\text{O}_2)(\text{Me}_2\text{-tpa})(\text{Me-tpa-CH}_2\text{OO})]^{2+}$ (m/z 407.60), and a bis(μ -alkylperoxo)dinickel(II) species, $[\text{Ni}_2(\text{Me-tpa-CH}_2\text{OO})_2]^{2+}$ (m/z 407.10). The former two species seem to be generated under ESI-TOF/MS conditions. Such a mononuclear species was also observed for the ESI-TOF/MS spectrum of $3^{\text{Me}_3\text{-tpa}}$.¹⁷ However, there is a possibility that the dissociation occurs only under the ESI-TOF/MS conditions.

To investigate the solution behavior of $[\text{Ni}_2(\text{O}_2)_2(\text{Me}_2\text{-tpa})_2]^{2+}$ (**3**) in acetonitrile, we characterized the nickel coordination spheres of both solution and solid samples by X-ray absorption spectroscopy. The Ni EXAFS of a frozen solution sample of **3** is quite similar to that of a solid sample, indicating that the $\text{Ni}^{\text{II}}(\mu\text{-OO})_2\text{Ni}^{\text{II}}$ core structure remains intact in solution, as shown in Figure 6 and Table 3. The nickel ligations for both samples consist of two oxygen

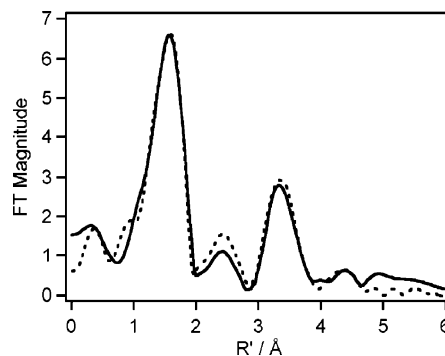


Figure 6. Fourier transform of EXAFS data of a frozen acetonitrile solution (solid line) and a solid sample (dashed line) of **3** at 100 K .

Table 3. Fitting Results of EXAFS Data for a Frozen Acetonitrile Solution of **3** and a Solid Sample of **3** at 100 K

		CN	R (\AA)	σ^2 ($\times 10^{-3}\text{ \AA}^2$)	R factor (%)
in frozen solution					
Ni–N	4 ^a		2.12 ± 0.03	7.5	4.8
Ni–O	2 ^a		1.92 ± 0.03	4.9	
Ni \cdots Ni	0.6 ± 0.5		3.75 ± 0.03	9.0	
in solid state					
Ni–N	4 ^a		2.11 ± 0.03	7.3	4.3
Ni–O	2 ^a		1.91 ± 0.03	5.2	
Ni \cdots Ni	0.7 ± 0.5		3.75 ± 0.03	9.2	

^a The values are fixed for the fittings. The k range for fitting is between 3 and 12 \AA^{-1} . The R range for the fittings is from 0.8 to 4.1 \AA . $R = \frac{\sum(k^m \chi_{\text{obs}} - k^m \chi_{\text{calcd}})^2}{\sum(k^m \chi_{\text{obs}})^2}$.

scatterers at short distance Ni–O_{ave} = 1.91 – 1.92 \AA , four nitrogen scatterers at Ni–N_{ave} = 2.11 – 2.12 \AA , and a nickel scatterer at 3.75 \AA , which are comparable to those of the crystal structure (Ni–O_{ave} = 1.947 \AA , Ni–N_{ave} = 2.100 \AA , and Ni \cdots Ni = $3.838(1)\text{ \AA}$). The energy of the absorption edge of a solution sample of **3** (8346 eV) is consistent with the Ni(II) oxidation state and is identical to that of a solid sample of **3** (8346 eV) (see the Supporting Information, Figure S5). Thus, the dimer structure of **3** remains intact in acetonitrile. This is also confirmed by the electronic spectral measurements. The electronic spectrum of **3** in acetonitrile at $-40\text{ }^{\circ}\text{C}$ showed a distinct absorption band at 335 nm ($\epsilon \approx 11\,000\text{ M}^{-1}\text{ cm}^{-1}$) and several d–d bands in the visible and near-infrared regions that are almost the same as those of the reflectance spectrum of a powdered sample prepared from crystals, as shown in panels b and c of Figure 3, which is in line with the EXAFS results.

The EPR spectrum of a frozen acetonitrile solution of **3** measured at 4.3 K exhibits a rhombic signal with g values of 2.22 , 2.18 , and 2.05 in the $\Delta m_s = 1$ region with a weak $\Delta m_s = 2$ signal at half-field, as shown in Figure 7. Five superhyperfine lines due to interaction with two nitrogens are observed on the $g = 2.05$ signal in the spectrum measured at 77 K . The spectral feature in the $\Delta m_s = 1$ region is quite similar to that observed for a recently characterized monomeric Ni(II)–superoxo complex $[\text{PhTt}^{\text{Ad}}]\text{Ni}(\text{O}_2)$ with a side-on superoxo ligand ($g = 2.24$, 2.19 , and 2.01).¹⁹ Each Ni(II) ion of **3** has two unpaired electrons in $d_{x^2-y^2}$ and d_z^2 orbitals. The electrons in two $d_{x^2-y^2}$ orbitals in Ni(II) ions and those in π^* orbitals of two O_2^- are antiferromagnetically coupled to yield an $S = 1/2$ ground state/Ni(II). Presence of the $\Delta m_s = 2$ signal at half-field for **3** clearly indicates that the dimer

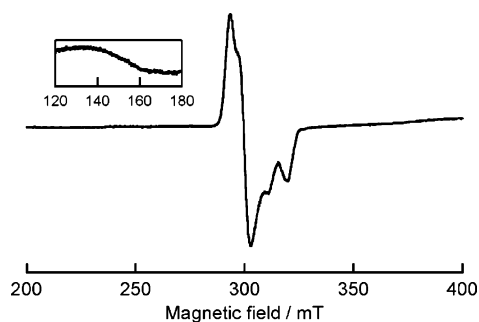


Figure 7. EPR spectrum of **3** (g values = 2.22, 2.18, 2.05) recorded at 4.3 K in acetonitrile. Inset is a spectrum in the half-field region. Spectral conditions: microwave power = 0.998 mW and modulation amplitude = 0.6 mT.

structure remains intact and each nickel(II) center has an unpaired electron in the d_{z^2} orbital and the interaction of the electrons yield a triplet state with a small zero-field splitting. A similar spectral feature is also observed for $3^{\text{Me}_3\text{-tpa}}$ (see the Supporting Information, Figure S6).

Reactivity of 2 and 3. Thermal decomposition of $[\text{Ni}_2(\text{O})_2(\text{Me}_2\text{-tpa})_2]^{2+}$ (**2**) in acetonitrile under N_2 at room temperature gave an N-dealkylated ligand ((6-methyl-2-pyridylmethyl)(2-pyridylmethyl)amine; 18% on the basis of the total amount of $\text{Me}_2\text{-tpa}$ ligand),³² a coupling dimer of $\text{Me}_2\text{-tpa}$ ligand ($(\text{Me-tpa-CH}_2)_2$; 26%),³³ a ligand-based carboxylate (Me-tpa-COO^- ; 13%), a hydroxylated ligand ($\text{Me-tpa-CH}_2\text{OH}$; 5%), and a trace amount of a ligand-based aldehyde (Me-tpa-CHO) which was detected by ^1H NMR and ESI-TOF/MS. Hereafter, the amount of modified ligands are reported on the basis of the total amount of $\text{Me}_2\text{-tpa}$ ligand. It is probable that Me-tpa-COO^- and $\text{Me-tpa-CH}_2\text{-OH}$ are not derived from oxidation of the methyl group in **2**, because as mentioned already, complex **2** contains some amount of complex **4** as an impurity, which can generate those two species. The formation of the N-dealkylated ligand and $(\text{Me-tpa-CH}_2)_2$ indicates that oxidation occurs both at the methyl and methylene groups. The formation of the coupling dimer clearly indicates the formation of a ligand-based radical ($\text{Me-tpa-CH}_2^\bullet$), which is stable enough for coupling with another $\text{Me-tpa-CH}_2^\bullet$. To investigate the formation mechanism of $(\text{Me-tpa-CH}_2)_2$, we examined the decomposition of a mixture of $[\text{Ni}_2(\text{O})_2(\text{Me}_2\text{-tpa})_2]^{2+}$ (**2**) and a complex with deuterated $d_1\text{-Me}_2\text{-tpa}$ ligands $[\text{Ni}_2(\text{O})_2(d_1\text{-Me}_2\text{-tpa})_2]^{2+}$ (**2-d**₁); the ESI-TOF/MS spectrum (Figure 8) revealed that the isotope pattern of the coupling dimers consists of only two isotopomers, $(\text{Me-tpa-CH}_2)_2$ and $d_2\text{-(Me-tpa-CH}_2)_2$, but not $d_1\text{-(Me-tpa-CH}_2)_2$, indicating that only an intramolecular ligand coupling occurs. Thus, the result indicates the formation of a bis($\text{Me-tpa-CH}_2^\bullet$) species

(32) This value corresponds to 40% oxidation yield on the basis of a bis(μ -oxo)dinickel(III) complex, because oxidative N-dealkylation corresponds to two-electron oxidation and a bis(μ -oxo)dinickel(III) complex is a two-electron oxidant.

(33) Reinvestigation of the decomposition of $3^{\text{Me}_3\text{-tpa}}$ revealed that $3^{\text{Me}_3\text{-tpa}}$ can also generate a coupling dimer ($\text{Me}_2\text{-tpa-CH}_2$)₂ together with $\text{Me}_2\text{-tpa-CH}_2\text{OH}$ depending on the reaction conditions, although we have reported that $3^{\text{Me}_3\text{-tpa}}$ generates only $\text{Me}_2\text{-tpa-CH}_2\text{OH}$ in ref 17. However, it was difficult to identify the reaction conditions. Further investigation is in progress.

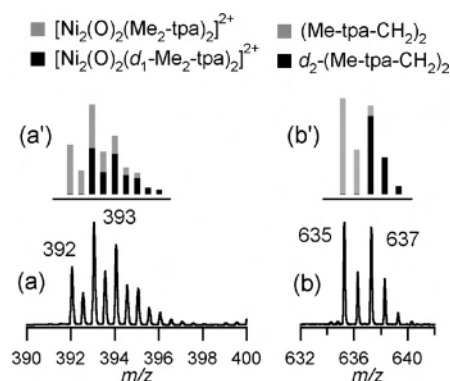


Figure 8. ESI-TOF/MS spectra of (a) the mixture of $[\text{Ni}_2(\text{O})_2(\text{Me}_2\text{-tpa})_2]^{2+}$ (**2**) and $[\text{Ni}_2(\text{O})_2(d_1\text{-Me}_2\text{-tpa})_2]^{2+}$ (**2-d**₁) in acetonitrile at -40 °C (relative intensity ratio **2**:**2-d**₁ = 52:48); and (b) coupling dimers in acetonitrile containing a small amount of HCOOH recovered after thermal decomposition of the above mixture at room temperature (relative intensity ratio $(\text{Me-tpa-CH}_2)_2:d_2\text{-(Me-tpa-CH}_2)_2$ = 55:45). No measurable $d_1\text{-(Me-tpa-CH}_2)_2$ is detected.

($[\text{Ni}_2(\text{OH})_2(\text{Me-tpa-CH}_2^\bullet)_2]^{2+}$) that is probably generated by stepwise H-atom abstractions from two methyl groups.

Thermal decomposition of **2** in acetonitrile at room temperature under O_2 gave an N-dealkylated ligand (18%), Me-tpa-COO^- (38%), and $\text{Me-tpa-CH}_2\text{OH}$ (12%). However, the coupling dimer, $(\text{Me-tpa-CH}_2)_2$, was not detected, indicating that the reaction of $\text{Me-tpa-CH}_2^\bullet$ with O_2 is much faster than the reaction between $\text{Me-tpa-CH}_2^\bullet$ radicals. Formations of Me-tpa-COO^- (38%) and $\text{Me-tpa-CH}_2\text{OH}$ (12%) are substantially larger than those obtained under N_2 , indicating that most of them are generated from **2** but not derived solely from **4**, which was present as an impurity. The ESI-TOF/MS spectrum of a decomposed sample of **2** under $^{18}\text{O}_2$ indicated that Me-tpa-COO^- contains $\text{Me-tpa-C}^{16}\text{O}^{16}\text{O}^-$, $\text{Me-tpa-C}^{16}\text{O}^{18}\text{O}^-$, and $\text{Me-tpa-C}^{18}\text{O}^{18}\text{O}^-$ in a 61:29:10 ratio and $\text{Me-tpa-CH}_2\text{OH}$ contains ca. 50% $\text{Me-tpa-CH}_2^{18}\text{OH}$, suggesting that they are derived from decomposition of the $\text{Me-tpa-CH}_2\text{OO}^\bullet$ species and/or autoxidation by dioxygen. It is noted that the ESI-TOF/MS spectrum of a sample decomposed under $^{18}\text{O}_2$ at -40 °C revealed the formation of $[\text{Ni}_2(\text{OH})(\text{Me}_2\text{-tpa})(\text{Me-tpa-CH}_2^{18}\text{O}^{18}\text{O})]^{2+}$ (**4- $^{18}\text{O}_2$**) (see the Supporting Information, Figure S7), indicating that **4** can be derived from **2** via the formation of $\text{Me-tpa-CH}_2\text{OO}^\bullet$, although quantitative analysis of **4** cannot be made at the present time. Complex **4** is capable of producing Me-tpa-COO^- and $\text{Me-tpa-CH}_2\text{OH}$ by decomposition (vide infra). In addition, $\text{Me-tpa-CH}_2\text{OO}^\bullet$ could generate $\text{Me-tpa-CH}_2\text{OH}$ and Me-tpa-CHO by the Russell termination, both of which are susceptible to autoxidation that generates carboxylate. Me-tpa-CHO is also capable of producing Me-tpa-COO^- and $\text{Me-tpa-CH}_2\text{OH}$ by the Cannizzaro reaction (vide infra).

Thermal decomposition of **3** in acetonitrile at -40 °C resulted in formation to **2** and O_2 , and at -20 °C, further oxidation generated **4**, although the yield of **4** is not known at present. We have also studied thermal decomposition of **3** at room temperature under N_2 . Yields of modified ligands recovered are N-dealkylated ligand (20%), $(\text{Me-tpa-CH}_2)_2$ (10%), Me-tpa-COO^- (18%), $\text{Me-tpa-CH}_2\text{OH}$ (18%), and Me-tpa-CHO (~4%). The presence of $(\text{Me-tpa-CH}_2)_2$ indi-

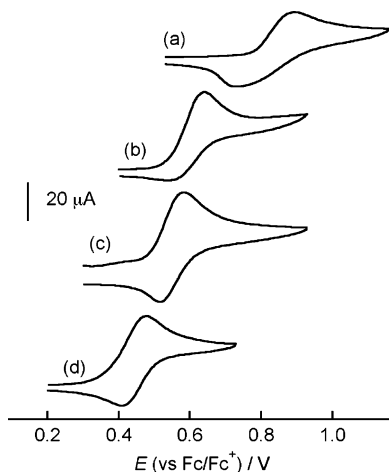


Figure 9. Cyclic voltammograms of (a) $1^{\text{Me}_3\text{-tpa}}$, (b) **1**, (c) $1^{\text{Me-tpa}}$, and (d) 1^{tpa} in acetonitrile (1 mM) containing 0.1 M $n\text{-Bu}_4\text{NClO}_4$ at -40°C (working electrode, Pt; reference electrode, Ag/Ag⁺; scan rate, 100 mV).

Table 4. Electrochemical Data for the Oxidation of Bis(μ -hydroxo)dinickel(II) Complexes in Acetonitrile at -40°C at Scan Rate = 0.1 V

complex	$E_{1/2}(\text{II,III/II,II})$ (ΔE) vs Fc/Fc ⁺ (V)
$[\text{Ni}_2(\text{OH})_2(\text{tpa})_2]^{2+}$ (1^{tpa})	0.45 (0.07)
$[\text{Ni}_2(\text{OH})_2(\text{Me-tpa})_2]^{2+}$ ($1^{\text{Me-tpa}}$)	0.55 (0.06)
$[\text{Ni}_2(\text{OH})_2(\text{Me}_2\text{-tpa})_2]^{2+}$ (1)	0.62 (~0.10)
$[\text{Ni}_2(\text{OH})_2(\text{Me}_3\text{-tpa})_2]^{2+}$ ($1^{\text{Me}_3\text{-tpa}}$)	0.78 (~0.16)

icates that the dioxygen concentration generated by the disproportionation of the superoxo ligands in **3** is not high enough for full formation of the Me-tpa-CH₂OO[•] species. Decomposition of **3** under O₂ at room temperature caused an increase in the formation of Me-tpa-COO⁻ (44%) and a decrease in the formation of Me-tpa-CH₂OH (11%) along with the N-dealkylated ligand (18%), probably suggesting that autoxidation of Me-tpa-CH₂OH and some other radical reactions take place under the experimental conditions.

Redox Behavior. The cyclic voltammogram (CV) of **1** in acetonitrile showed a quasireversible redox couple at $E_{1/2} = 0.62$ V vs Fc/Fc⁺ at a scan rate 100 mV s⁻¹, as shown in Figure 9b. Similar redox behavior has also been reported for the five-coordinate bis(μ -hydroxo)dinickel(II) complexes containing tridentate N-donor ligands ($E_{1/2} = 0.66\text{--}0.78$ V vs Fc/Fc⁺). The redox couples have been assigned to the one-electron oxidation of the Ni₂(II,II) state to the Ni₂(II,III) state.^{16b} The CV data of the bis(μ -hydroxo)dinickel(II) complexes with a series of tpa derivatives (tpa (1^{tpa}), Me-tpa ($1^{\text{Me-tpa}}$), Me₂-tpa (**1**), and Me₃-tpa ($1^{\text{Me}_3\text{-tpa}}$)) are given in Table 4. The data show that the successive introduction of the 6-methyl group into the pyridyl group of the tpa ligand causes a successive positive shift of $E_{1/2}$ - (Ni₂(II,III)/Ni₂(II,II)) values from 0.45 to 0.78 V. Such a positive shift is in line with the general trend that the 6-methyl group weakens the electron-donor ability of the pyridyl group because of the steric requirements, leading to destabilization of the high-valence oxidation state.^{9i,34}

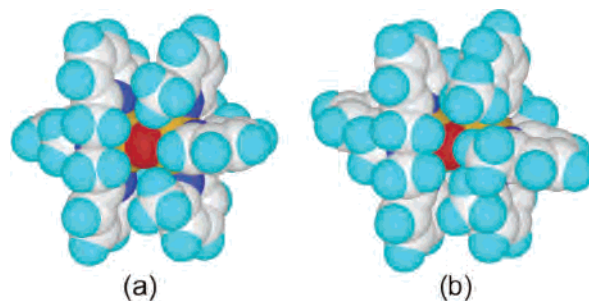


Figure 10. Comparison of space-filling models of (a) **2** and (b) $2^{\text{Me}_3\text{-tpa}}$ (nickel, yellow; oxygen, red; nitrogen, blue; carbon, gray; hydrogen, pale blue).

Discussion

The Me₂-tpa ligand forms the bis(μ -oxo)dinickel(III) **2** and bis(μ -superoxo)dinickel(II) **3** complexes as well as the Me₃-tpa ligand. Bis(μ -superoxo)dinickel(II) complexes are derived from the oxidation of H₂O₂ by bis(μ -oxo)dinickel(III) complexes. However, the reactivity of **2** with H₂O₂ is quite different from that of $[\text{Ni}_2(\text{O})_2(\text{Me}_3\text{-tpa})_2]^{2+}$ ($2^{\text{Me}_3\text{-tpa}}$). Unlike $2^{\text{Me}_3\text{-tpa}}$, complex **2** could not be obtained by direct reaction of $[\text{Ni}_2(\text{OH})_2(\text{Me}_2\text{-tpa})_2]^{2+}$ (**1**) with H₂O₂, because **2** is extremely reactive with H₂O₂ and produces **3**. This differential reactivity may be attributable to the structural features of **2** and $2^{\text{Me}_3\text{-tpa}}$ (Figure 10). Complex **2** has a space around the Ni^{III}(μ -O)₂Ni^{III} core for access of H₂O₂, whereas there is not enough space around the Ni^{III}(μ -O)₂Ni^{III} core in $2^{\text{Me}_3\text{-tpa}}$. Thus, the in-plane 6-methylpyridyl groups in $2^{\text{Me}_3\text{-tpa}}$ significantly suppress the reactivity with H₂O₂ by stereochemical effects. It is noted that bis(μ -oxo)dinickel(III) complexes with tridentate ligands such as bis[2-(2-pyridyl)ethyl]amine and Tp^{Me₃} have no reactivity with H₂O₂, although a space-filling model of the Tp^{Me₃} complex suggests that there is a space around the Ni^{III}(μ -O)₂Ni^{III} core for access of H₂O₂. It is also noted that the $E_{1/2}(\text{II,III/II,II})$ values (0.66–0.78 V) of the bis(μ -hydroxo)dinickel(II) complexes with tridentate ligands are comparable and/or more positive than those of the present complexes with tetradentate ligands,^{16b} suggesting that the former bis(μ -oxo)dinickel(III) complexes are stronger oxidants than the present bis(μ -oxo)dinickel(III) complexes. Although the differential reactivity between these two types of complexes is very interesting, the origin of this difference is not clear at present.

The 6-methyl groups of the pyridyl sidearms also have a significant influence on various physicochemical properties of the bis(μ -oxo)dinickel(III) complexes. Introduction of the 6-methyl group into the pyridyl group has been shown to weaken the electron-donor ability of the pyridyl nitrogen because of steric requirements, which destabilizes high-valence species, leading to a stronger oxidant. This is in line with the successive positive shift of the $E_{1/2}$ values of $[\text{Ni}_2(\text{OH})_2(\text{Me}_n\text{-tpa})_2]^{2+}$ (Table 4). Complex $2^{\text{Me}_3\text{-tpa}}$ decomposes within 1 h at -40°C , whereas **2** is stable over a day under the same conditions. The high reactivity of $2^{\text{Me}_3\text{-tpa}}$ may be partly due to the proximity effect between the in-plane methyl groups and the oxo groups and partly to the higher oxidation ability of $2^{\text{Me}_3\text{-tpa}}$.

(34) Gultneh, Y.; Yisgedu, T. B.; Tesema, Y. T.; Butcher, R. J. *Inorg. Chem.* **2003**, *42*, 1857.

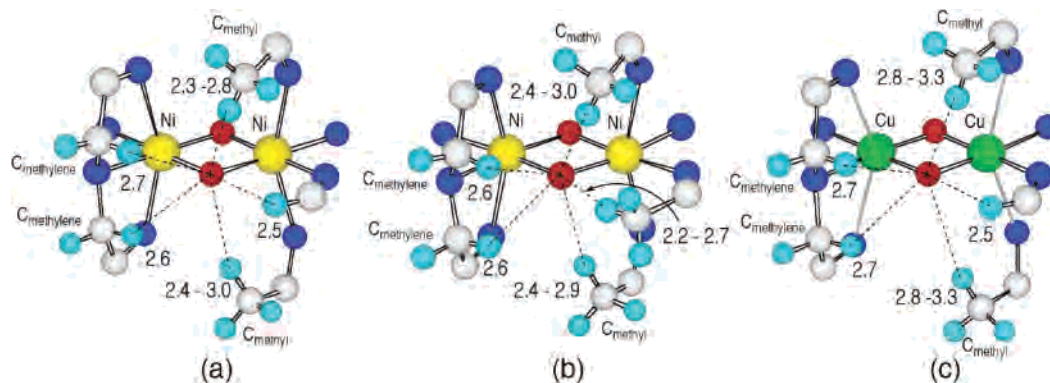
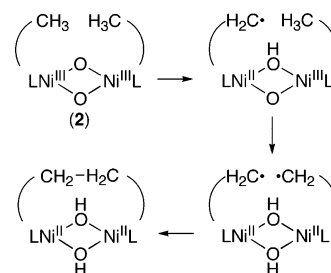


Figure 11. Chem3D models of (a) **2**, (b) $2^{\text{Me}_3\text{-tpa}}$, and (c) 2^{Cu} showing the $\text{H}\cdots\text{O}_{\text{oxo}}$ distances (Å) close to the oxo groups. Hydrogen atoms were placed at the calculated positions ($\text{C}-\text{H} = 0.95$ Å).

Although complex $2^{\text{Me}_3\text{-tpa}}$ almost selectively oxidizes the methyl group of $\text{Me}_3\text{-tpa}$,¹⁷ the present complex **2** can oxidize both methylene and methyl groups. This seems to be closely related to the structural features between the oxo groups and hydrogens of the methylene and methyl groups and their $\text{C}-\text{H}$ bond energies. A Chem3D model of **2** suggests that the $\text{O}_{\text{oxo}}\cdots\text{H}$ distances for the methyl groups are 2.3–3.0 Å, depending on the orientation of the hydrogen atoms of the methyl groups, and those for the methylene groups are 2.6–2.7 Å (Figure 11a). Although the hydrogens of the methyl groups can more closely approach the oxo groups, the oxidation of the methylene groups may be attributable to the weaker $\text{C}-\text{H}$ bond energy of the methylene groups. A similar N-dealkylation has also been observed for the corresponding copper complex $[\text{Cu}_2(\text{O})_2(\text{Me}_2\text{-tpa})_2]^{2+}$ (2^{Cu}), where no oxidation of the methyl group was detected.^{9f} A Chem3D model of 2^{Cu} reveals that the $\text{O}_{\text{oxo}}\cdots\text{H}$ distances for the axial methyl groups (2.8–3.3 Å) are longer than those in **2** as shown in Figure 11c. Thus, the hydrogen atoms of the methyl groups in **2** can more closely approach the oxo group compared to those in 2^{Cu} and this seems to be responsible for the parallel oxidation of the methyl and methylene groups. In contrast, selective oxidation of the methyl group was observed for $2^{\text{Me}_3\text{-tpa}}$ (only a trace amount of N-dealkylation was detected), which seems to be due to the proximity effect of the in-plane methyl group in $2^{\text{Me}_3\text{-tpa}}$ ($\text{O}_{\text{oxo}}\cdots\text{H} = 2.2\text{--}2.7$ Å).

Decomposition of **2** under N_2 gave a ligand-based coupling dimer $(\text{Me-tpa-CH}_2)_2$, indicating the formation of a ligand-based radical ($\text{Me-tpa-CH}_2^\bullet$) that was probably generated by H-abstraction of the methyl group of $\text{Me}_2\text{-tpa}$, as found for various high-valence $\text{M}(\text{III})_2(\mu\text{-O})_2$ complexes ($\text{M} = \text{Cu, Ni, and Co}$).^{6,14,16} However, oxygen rebound is slow in **2**,³⁵ and the resulting ligand-based radical ($\text{Me-tpa-CH}_2^\bullet$) is stable enough for coupling with another $\text{Me-tpa-CH}_2^\bullet$. The isotope-labeling experiment using a mixture of $[\text{Ni}_2(\text{O})_2(\text{Me}_2\text{-tpa})_2]^{2+}$ (**2**) and $[\text{Ni}_2(\text{O})_2(d_1\text{-Me}_2\text{-tpa})_2]^{2+}$ (**2-d₁**) clearly indicates that bis($\text{Me-tpa-CH}_2^\bullet$)dinickel(II) species ($[\text{Ni}_2(\text{OH})_2(\text{Me-tpa-CH}_2)_2]^{2+}$ and $[\text{Ni}_2(\text{OH})_2(d_1\text{-Me-tpa-CH}_2)_2]^{2+}$) are generated

Scheme 2

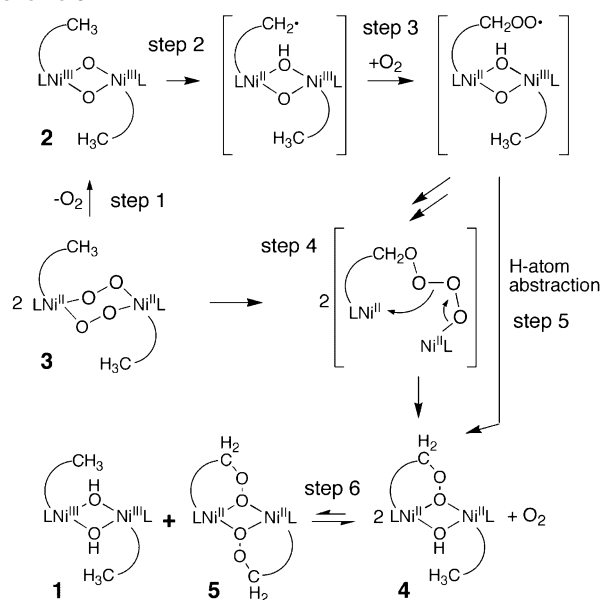


and only an intramolecular coupling occurs, where the bis($\text{Me-tpa-CH}_2^\bullet$) species could be generated by stepwise H-atom abstractions from two methyl groups (Scheme 2). Decompositions of the bis($\mu\text{-oxo}$)dinickel(III) complex **2** and bis($\mu\text{-superoxo}$)dinickel(II) complex **3** under O_2 produced no coupling dimer, clearly indicating that the ligand-based radical, $\text{Me-tpa-CH}_2^\bullet$, is very reactive to dioxygen and the reaction is much faster than the coupling of $\text{Me-tpa-CH}_2^\bullet$ radicals and the oxygen rebound.

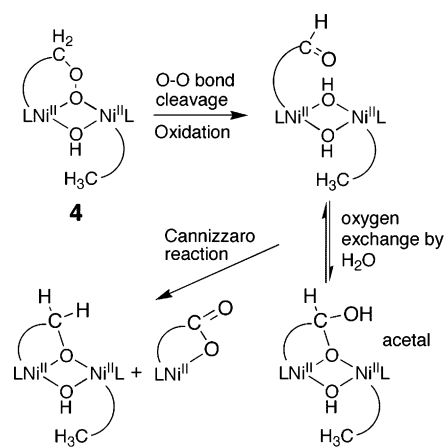
Decomposition of **2** and **3** under O_2 at room temperature produced the ligand-based carboxylate (Me-tpa-COO^- , yield $\approx 38\text{--}44\%$), alcohol ($\text{Me-tpa-CH}_2\text{OH}$, yield $\approx 12\%$), and a trace amount of aldehyde (Me-tpa-CHO) together with the N-dealkylated ligand (yield $\approx 20\%$). The oxidation product of the methyl groups of the $\text{Me}_2\text{-tpa}$ ligand could be mainly produced from the peroxy radical ($\text{Me-tpa-CH}_2\text{OO}^\bullet$), as mentioned already. The oxidation reaction seems to involve some complicated reactions such as radical chain reactions and autoxidation. However, one of the reactive intermediates that can generate the oxidation products (Me-tpa-CHO , Me-tpa-COO^- , and $\text{Me-tpa-CH}_2\text{OH}$) was identified and isolated during decomposition of **3** under O_2 at -20 °C. ESI-TOF/MS measurement showed the formation of the ligand-based monoalkylperoxo complex ($[\text{Ni}_2(\text{OH})(\text{Me}_2\text{-tpa})(\text{Me-tpa-CH}_2\text{OO})]^{2+}$ (**4**)), as shown in Figure 1. A possible conversion pathway is given in Scheme 3, which consists of the following steps: step (1) disproportionation of the superoxo ligands in **3** gives O_2 and **2**; step (2) **2** generates a ligand-based alkyl radical ($\text{Me-tpa-CH}_2^\bullet$); step (3) the resulting $\text{Me-tpa-CH}_2^\bullet$ reacts with O_2 to produce a ligand-based alkylperoxy radical ($\text{Me-tpa-CH}_2\text{OO}^\bullet$); step (4) coupling between $\text{Me-tpa-CH}_2\text{OO}^\bullet$ and a superoxo ligand of **3** and its rearrangement gave **4** and O_2 . In addition to this pathway, step (5) H-atom abstraction by $\text{Me-tpa-CH}_2\text{OO}^\bullet$ species may

(35) As mentioned already, although a hydroxylated ligand, $\text{Me-tpa-CH}_2\text{-OH}$, was recovered, it is not clear at present whether $\text{Me-tpa-CH}_2\text{OH}$ is derived from $[\text{Ni}_2(\text{OH})(\text{Me}_2\text{-tpa})(\text{Me-tpa-CH}_2\text{OO})]^{2+}$ (**4**) present as an impurity or rebound of oxygen. Even if $\text{Me-tpa-CH}_2\text{OH}$ is generated by a rebound mechanism, this seems to not be significant for **2**.

Scheme 3



Scheme 4



also be involved, as mentioned already. Complex **5** can be generated by the disproportionation of **4**, and **1** generated simultaneously may further react with H_2O_2 to generate **5** in the same way.

Previously, we reported that the bis(μ -alkylperoxy)-nickel(II) complex (**5**) gave oxidation products Me-tpa-COO⁻ (62%) and Me-tpa-CH₂OH (37%) upon decomposition under Ar. They may be produced by the stepwise reactions shown in Scheme 4, which involves the conversion of the peroxy ligand into a ligand-based aldehyde by either homolysis or heterolysis of the O–O bond and disproportionation of the aldehyde to give carboxylate and alkoxide via the Cannizzaro reaction. Although this oxidation pathway gives equal amounts of Me-tpa-COO⁻ and Me-tpa-CH₂OH, the observed high yield of the carboxylate ligand compared to that of the alkoxide ligand suggests that some other side reactions take place at the same time.

In summary, a series of the sequential reaction intermediates for the oxidation of the Me₂-tpa supporting ligand of **1**

by reaction with H_2O_2 , **2**, **3**, and **4** was successfully isolated and characterized by various physicochemical techniques. The crystal structures, formation processes, and ligand oxidation reactions provide some fundamental insights into their reactivities.

Complex **2** is extremely reactive with H_2O_2 , compared to **2**^{Me₃-tpa}. This is attributable to a lack of the in-plane 6-methylpyridyl group, which allows H_2O_2 to react with the bis(μ -oxo) core. In contrast, **2**^{Me₃-tpa} is very unstable compared to **2**. This is due to a high reactivity of the oxo group toward the supporting ligand in **2**^{Me₃-tpa}.

Complex **2** is capable of oxidizing both methyl and methylene groups, whereas **2**^{Me₃-tpa} and **2**^{Cu} selectively oxidize the methyl group and the methylene group, respectively. Such differential reactivity is ascribed to the proximity effect between H atoms and the oxo groups along with the C–H bond energies.

Oxidation of the methyl group starts from the formation of the ligand-based radical (Me-tpa-CH₂[•]). However, oxygen rebound observed for various high-valence bis(μ -oxo)dimetal complexes is slow enough to allow intramolecular coupling of Me-tpa-CH₂[•] under N₂. The isotope-labeling experiment clearly indicates that the bis(Me-tpa-CH₂[•]) species ([Ni₂(OH)₂(Me-tpa-CH₂[•])₂]²⁺) is generated and only an intramolecular coupling occurs, where the bis(Me-tpa-CH₂[•]) species could be generated by stepwise H-atom abstractions from two methyl groups.

Under O₂, Me-tpa-CH₂[•] reacts with O₂ to generate Me-tpa-CH₂OO[•], which undergoes further oxidation to give Me-tpa-COO⁻ and Me-tpa-CH₂OH as the final products. Decomposition reactions of **2** and **3** seem to involve various pathways, such as radical chain reactions and autoxidation. However, one of the reactive intermediates was identified as the alkylperoxy species **4**, which may be derived from coupling between Me-tpa-CH₂OO[•] and a superoxo ligand of **3**, and its rearrangement gave **4** and O₂. In addition, H-atom abstraction by Me-tpa-CH₂OO[•] seems to be possible for the formation of the alkylperoxy ligand.

The bis(μ -alkylperoxy)nickel(II) complex **5** obtained by the reaction of **1** with excess of H_2O_2 at $-20\text{ }^\circ\text{C}$ gave Me-tpa-COO⁻ and Me-tpa-CH₂OH. They are derived from stepwise reactions, which involve the conversion of the peroxy ligand into a ligand-based aldehyde by O–O bond cleavage and disproportionation of the aldehyde to give carboxylate and alkoxide via the Cannizzaro reaction.

Acknowledgment. This work was partly supported by Grants-in-Aid for Scientific Research from the Ministry of Education, Science, and Culture, Japan (M.S., H.F., and T.K.).

Supporting Information Available: Listings of Figure S1–S9 and three X-ray crystallographic files in CIF format. This material is available free of charge via the Internet at <http://pubs.acs.org>.

IC0514243